

THE CAUSES FOR TEMPERATURE
FLUCTUATIONS ON CATALYTIC WIRES

A Thesis
Presented to
The Faculty of the
Chemical Engineering Department
University of Houston
Houston, Texas

In Partial Fulfillment
of the Requirements for the Degree of
Master of Science in Chemical Engineering

By
Jorge E. Zuñiga-Chaves
May, 1974

ACKNOWLEDGMENTS

I would like to express my sincere appreciation to Dr. Dan Luss for his guidance, continuous interest and friendly criticism throughout the course of this work. The candid observations and suggestions made by Dr. Frank L. Worley, Jr. were most helpful for the completion of this study.

Among the many friends who have helped me in this work I take pleasure in acknowledging the assistance of Dr. William M. Edwards who patiently taught me most of the experimental techniques discussed in Chapter IV.

Finally, this project would have not been possible without the encouragement and moral support of my wife Erika. To her and my daughter Barbara this work is dedicated.

THE CAUSES FOR TEMPERATURE
FLUCTUATIONS ON CATALYTIC WIRES

An Abstract of a Thesis
Presented to
the Faculty of the
Chemical Engineering Department
University of Houston
Houston, Texas

In Partial Fulfillment
of the Requirements for the Degree of
Master of Science in Chemical Engineering

By
Jorge E. Zúñiga-Chaves
May, 1974

ABSTRACT

Random temperature fluctuations can be observed on the surface of catalytic wires when an exothermic mass transfer limited chemical reaction takes place on them. In industrial reactors, these large magnitude temperature fluctuations (flickering) have a deleterious influence on the rate of metal loss from the gauzes.

An experimental investigation was undertaken to determine the main causes of flickering. The surface temperature fluctuations on single platinum wires were measured with an infrared detector during the oxidation of hydrogen or ammonia in excess air.

Independent measurements of turbulence intensity and concentration fluctuations in the gaseous mixture were made. The rms amplitude of the latter was measured by means of an aspirating probe.

The characteristic time for wire temperature changes was much greater than the characteristic time for changes in surface concentration for these reaction experiments. The results indicate that concentration fluctuations due to incomplete mixing of the reactants are the main cause of the temperature fluctuations.

TABLE OF CONTENTS

CHAPTER	PAGE
I. INTRODUCTION	1
II. THEORETICAL CONSIDERATIONS	5
A. The Exothermic Chemical Reaction	5
B. The Pseudo-Steady State Model	8
C. Electrically Heated Wires	12
1) Temperature distribution	12
2) Constant temperature measurements of velocity fluctuations	14
3) Reaction and constant temperature measurements of concentration fluctuations .	17
D. Random Stationary Processes	20
E. Turbulent Flow Properties	23
F. Spectra Relations for Reacting Wires	25
III. EXPERIMENTAL SYSTEM	27
A. General Description	27
B. Flow Channel	29
C. Air, Nitrogen and Reactants Supply	31
D. Wire Support Probes	32
E. Aspirating Probe	34
F. Infrared Thermal Microplotter	36
G. Measuring and Recording Equipment	39

CHAPTER	PAGE
IV. EXPERIMENTAL TECHNIQUES	43
A. General Procedure	43
B. Wire Temperature Calibration and Measurements .	45
C. Turbulence Measurements	47
D. Concentration Fluctuations Measurements	48
1) Aspirating probe procedure	48
2) Constant temperature procedure	49
V. EXPERIMENTAL RESULTS	51
A. Preliminary Experiments	51
B. Measurement of Hydrogen Concentration Fluctuations	52
C. Hydrogen-Air Reaction	56
D. The Pseudo-Steady State Test	56
E. Probability Density Functions	61
F. Effect of Wire Diameter	64
G. Power Spectral Density Functions	68
H. Ammonia Air Experiments	78
I. Constant Temperature Experiments	81
VI. CONCLUSIONS AND RECOMMENDATIONS	86
NOMENCLATURE	88
BIBLIOGRAPHY	93

APPENDIX I	Calibration of Experimental Equipment .	94
APPENDIX II	Turbulence Intensity Determination For Constant Temperature Operation (hot-wire sensor)	100
APPENDIX III	Derivation of Eq. (2-16) and Eq. (2-56) When the Lewis Number is Different From Unity	104

LIST OF FIGURES

FIGURE		PAGE
3.1	Schematic of the overall test assembly	28
3.2	Schematic of the flow channel	30
3.3	Catalytic wire probe	33
3.4	Aspirating probe diagram	35
3.5	Schematic of infrared thermal microplotter ...	38
3.6	Measuring and recording equipment	41
5.1	Effect of the injection angle on the concentration fluctuations amplitude ($N_{Re} = 4000, T_g = 24^\circ C$)	53
5.2	Concentration profile at the wire station ($N_{Re} = 4000, x_g = .025$)	55
5.3	Effect of the injection angle on the temperature fluctuations ($N_{Re} = 4000,$ $d_w = .075 \text{ mm}, T_g = 24^\circ C$)	57
5.4	Effect of the angular position of the distributor on τ_c ($N_{Re} = 4000, T_g = 24^\circ C$)	59
5.5	Effect of the injection angle on $\langle x_g \rangle$ and $c'_{rms}/\langle c \rangle; T'_{rms}/\langle T_c - T_g \rangle$ for a 0.075 mm wire and on $c'_{rms}/\langle c \rangle$ computed from Eq. (5-1) .	60

5.6 Probability density function of hydrogen concentration fluctuations ($N_{Re} = 4000$, $T_g = 24^\circ\text{C}$) 62

5.7 Probability density function of temperature fluctuations ($N_{Re} = 4000$, $T_g = 24^\circ\text{C}$, $d_w = 0.075$ mm) 63

5.8 Probability density function of air turbulence ($T_g = 24^\circ\text{C}$) 65

5.9 a) Effect of wire diameter and position of distributor on the temperature fluctuations for a mixture of 2.5% vH₂ in air
 b) Computed values of $c'_{rms}/\langle c \rangle$ from $T'_{rms}/\langle T_c - T_g \rangle$ using equation (5-1)..... 67

5.10 Normalized spectral density function of temperature fluctuations during hydrogen oxidation ($d_w = 0.025$ mm, $\phi = 180^\circ$, $x_g = .025$, $T_g = 24^\circ\text{C}$) 69

5.11 Normalized spectral density function of temperature fluctuation during the oxidation of either hydrogen or ammonia in air ($\tau_c = 0.030$ sec, $N_{Re} = 4000$, $T_g = 24^\circ\text{C}$) 71

5.12 Normalized spectral density function of temperature fluctuations during hydrogen oxidation ($d_w = .075$ mm, $\phi = 180^\circ$, $x_g = .025$, $T_g = 24^\circ\text{C}$) 72

5.13	Normalized power spectrum of temperature fluctuations during hydrogen oxidation ($x_g = .025$, $d_w = .025$ mm, $N_{Re} = 4000$ $T_g = 24^\circ\text{C}$)	74
5.14	Power spectral density of hydrogen concen- tration fluctuations ($N_{Re} = 4000$, $x_g = .025$, $T_g = 24^\circ\text{C}$).....	76
5.15	Power spectral density of hydrogen concen- tration and pressure fluctuations ($N_{Re} = 4000$, $T_g = 24^\circ\text{C}$)	77
5.16	Effect of the angular position and size of the holes of the distributor on the magnitude of $T'_{rms}/\langle T_c - T_g \rangle$ and $\langle \Delta T_{ad}^* \rangle$ for ammonia oxidation ($d_w = 0.075$ mm, $T_g = 24^\circ\text{C}$)	80
5.17	Correlation of electrical overheat results for constant temperature operation according to the pseudo-steady state model	83
I.1	Air flowmeter calibration ($T_g = 24^\circ\text{C}$)	95
I.2	Hydrogen flowmeter calibration (1/4 CD float).	98
I.3	Helium flowmeter calibration (1/4 CD float)...	99

LIST OF TABLES

TABLE		PAGE
2.1	Computed values of N_{Le} and K (Ref. [4])	8
5.1	Calculated and measured hydrogen fluctuations.	58
5.2	Calculated hydrogen fluctuations for $\phi = 180^\circ$ ($\tau_c = 0.039$ sec)	66
5.3	Calculated hydrogen fluctuations for $\phi = 270^\circ$ ($\tau_c = 0.030$ sec).....	66
5.4	Hydrogen fluctuation $c'_{rms}/\langle c \rangle$ evaluated by three different methods ($x_g = 0.025$)	82
5.5	Experimental values of R_{uc} for hydrogen oxidation	85

CHAPTER I
INTRODUCTION

Some chemical processes of industrial importance, such as the oxidation of ammonia to nitric acid and the production of hydrogen cyanide, are carried out commercially over catalytic gauzes. In these reactors, several layers of platinum-rhodium gauzes are packed together and contacted with a fast flowing stream of gases.

Observations of these catalytic screens during operation, shows that the luminosity of certain regions constantly fluctuates. The bright spots appear and decay in a random fashion and the phenomenon has been referred to as "flickering".

It is believed that these temperature fluctuations influence the degree of surface roughness attained by the catalyst during the activation period. More important, however, is the influence of flickering on the rate of precious metal loss from the gauze.

Experimental data for the oxidation of ammonia^[1] yielded the following empirical correlation for the rate of metal loss

$$-\frac{dM}{dt} = f(O_2) \exp[-E_m/RT] \quad (1-1)$$

where $E_m \approx 40000$ cal/gr mole. Thus, the rate of deterioration of the gauze is a convex function of the temperature.

The influence of flickering on the metal loss can be estimated by defining a parameter $r(T)$ (relative metal loss). This parameter is the ratio between the metal loss with flickering (fluctuating temperature) to the metal loss during uniform temperature operation, at the same average temperature and oxygen concentration.

Thus, the relative metal loss can be expressed as

$$r(T) = \frac{\langle \frac{dM}{dt} \rangle}{\left(\frac{dM}{dt} \right)_{T=\langle T \rangle}} = \frac{\langle \exp\left(-\frac{E_m}{RT}\right) \rangle}{\exp\left(\frac{-E_m}{R\langle T \rangle}\right)} \quad (1-2)$$

where the symbol $\langle \rangle$ denotes the time average of a stationary quantity.

For a given value of the average operation temperature $\langle T \rangle$, the parameter $r(T)$ can be calculated at different intensities of root-mean-square (rms) temperature fluctuations. To accomplish this, however, the probability density function of the oscillations must be known.

Edwards^[4] has reported values of relative metal loss calculated under the assumption of a Gaussian distribution for the flickering, and typical operating conditions for ammonia-oxidation convertors.

The metal loss at a given average temperature increases considerably with an increase in the standard deviation (rms) of the temperature fluctuations. Therefore, it is of major importance

to reduce the magnitude of the flickering during commercial operations.

Very little information is available concerning the effect of flickering on the mechanical strength, activity and selectivity of catalytic gauzes. However, a model explaining the causes of this phenomenon would be a first step in gaining further insight about these important effects.

Ervin and Luss^[2] suggested that changes in the turbulent velocity fluctuations might be the cause for the large temperature oscillations observed on catalytic wires and gauzes. Experiments reported by Edwards, et al.^[3] indicated that a certain relation existed between flickering and turbulent velocity fluctuations.

Those experiments were carried out under conditions where the capacity term \underline{a} (defined by Equation (2-10) Chapter II) was large and, according to the model of Ervin and Luss^[2], in that case flickering should be negligible. Nevertheless, temperature fluctuations of significant magnitude were observed. In a later work^[4], it was shown that when the capacity term is large, temperature oscillations must be induced mainly by concentration fluctuations in the reaction mixture.

To further check this assertion, several experiments with single platinum wires were performed. In this work the results of these experiments are reported.

Measurements of temperature fluctuations during the oxidation of either hydrogen or ammonia in a turbulent air stream were made. A high resolution infrared unit was used to detect the temperature fluctuations on the surface of the wires during the reaction.

Different feed ports and methods of injection were used in order to obtain several levels of concentration fluctuations. The latter were measured by means of an aspirating probe.

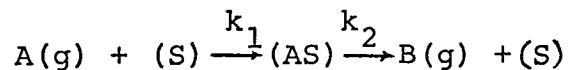
The statistical properties of both fluctuating quantities - concentration and temperature - were analyzed and compared to determine the major cause of flickering at various levels of fluctuations intensity.

CHAPTER II

THEORETICAL CONSIDERATIONS

A. The Exothermic Chemical Reaction

Consider the case^[5] of a catalytic wire of finite length on which a single chemical reaction occurs according to the mechanism



The following assumptions simplify the mass and energy balances.

- 1) Surface diffusion of the adsorbed species is negligible.
- 2) The catalytic activity is uniform along the length of the wire and does not change during the course of the reaction.
- 3) The rate of mass transfer and adsorption is $k_1(A)(S)$ where k_1 is independent of temperature and surface coverage.
- 4) Only a monolayer of adsorbed species is formed on the surface.
- 5) The surface reaction is first order and irreversible.

In addition to these five conditions, the supports of the wire are assumed to have no catalytic activity and are so large that their temperature is equal to that of the surrounding gas.

With the above assumptions the mass and energy balances become^[5]:

$$\frac{\partial (AS)}{\partial t} = k_1 (S) C_g - r \quad (2-1)$$

$$(AS) + (S) = L \quad (2-2)$$

$$A\rho C_p \frac{\partial T}{\partial t} = k_w A \frac{\partial^2 T}{\partial x^2} + hP(T_g - T) + (-\Delta H)P r \quad (2-3)$$

Subject to the boundary conditions

$$T = T_g \quad \text{at} \quad x = 0, \ell_w$$

If the wire is placed in a turbulent flow field where the heat and mass transfer coefficients as well as the temperature and composition of the fluid may fluctuate, a steady state can not be reached.

However, the wire can attain a stationary state whose statistical properties do not change with time. Under these conditions, the following time averaged relation must be satisfied.

$$k_w A \left\langle \frac{d^2 T}{dx^2} \right\rangle + P \langle h(T_g - T) \rangle + (-\Delta H) P \langle r \rangle = 0 \quad (2-4)$$

When the process is mass transfer controlled $(AS)/L$ is very small and $\langle r \rangle = \langle k_1 (S) C_g \rangle$ can be approximated by

$$\langle r \rangle = \langle k_c C_g \rangle \quad (2-5)$$

Substitution of (2-5) into Equation (2-4) yields

$$\langle h(T - T_g) \rangle = (-\Delta H) \langle k_c C_g \rangle + \frac{k_w A}{P} \left\langle \frac{d^2 T}{dx^2} \right\rangle \quad (2-6)$$

From this equation, it has been shown by Edwards, et al. [3], that the maximum temperature rise is given by

$$\langle \Delta T_{ad}^* \rangle = \langle \Delta T_{ad}^* \rangle + \frac{Ak_w}{P \langle h \rangle} \left\langle \frac{d^2 T}{dx^2} \right\rangle \quad (2-7)$$

where

$$\langle \Delta T_{ad}^* \rangle = \frac{(-\Delta H) C_g}{\rho_f C_{pf}} \left(\frac{N_{Pr}}{N_{Sc}} \right)^{2/3} = \frac{(-\Delta H) x_g}{C_{pf} M_f} (N_{Le})^{-2/3} \quad (2-8)$$

The second term on the RHS of Eq. (2-7) accounts for the influence of thermal conduction. It is negligible compared to $\langle \Delta T_{ad}^* \rangle$ for wires with a length to diameter ratio greater than 200.

Thus, for this condition, the adiabatic temperature rise can be estimated from physical and thermodynamic properties of the reacting gases and measuring the mole fraction of the limiting reactant in the stream surrounding the wire.

Edwards [4] has reported values of N_{Le} for different gases in excess air along with K , a constant to be used in Equation (2-8) in the form

$$\langle \Delta T_{ad}^* \rangle = K x_g \quad (2-9)$$

These values are shown in TABLE 1.

TABLE 1
 Computed values of N_{Le}
 and K (Ref. [4])

Reactant	N_{Le}	K [C°]
butane	2.30	47500
hydrogen	0.27	19600
ammonia	0.895	8000
methane	0.99	27400

B. The Pseudo-Steady State Model

Ervin and Luss^[2] used numerical simulations to show that large magnitude flickering could be induced by fluctuations in the transport coefficients. These temperature fluctuations were related to a new parameter, a , defined as

$$a = \frac{A \rho_p C_p \langle k_c \rangle \langle C_g \rangle}{\langle h \rangle L P} \quad (2-10)$$

This capacity term is the ratio of the characteristic time for temperature changes on the wire to the characteristic time for changes in the rate of mass transfer.

The results of these simulations indicated that the magnitude of the peak-to-peak temperature fluctuations decreased from about 200°C to almost 5°C as the parameter a was increased from 0.25 to 2. For values of a greater than 2, the simulated temperature fluctuations were completely negligible.

The capacity term can also be written as

$$a = \frac{A \rho C_p \langle \Delta T_{ad}^* \rangle}{L P (-\Delta H)} \quad (2-11)$$

where all the quantities, with the exception of L, can be measured for a given chemical reaction.

In order to predict a lower bound on the capacity term, Edwards^[4] estimated an upper bound on the concentration of active surface sites (L) and used the extinction concentration in Eq. (2-9) to evaluate $\langle \Delta T_{ad}^* \rangle$. The ratio A/P in Eq. (2-11) was computed for $d_w = 0.025$ mm which is a typical lower bound on the diameter of catalytic wires used in practice.

The calculations indicated that for the oxidation of either hydrogen or ammonia in excess air, the value of a was several hundred times greater than 2. Thus, for the experiments described in this work, the model of Ervin^[2] can not be used to explain the observed temperature fluctuations.

An alternate model has been proposed by Edwards^[4] based mainly on the following assumptions:

- 1) The reaction is mass transfer limited.
- 2) The capacity term is large.
- 3) The temperature, the composition of the gas and the transport coefficients may fluctuate.

When the capacity term a is large, the pseudo-steady state approximation applies and Eq. (2-1) becomes

$$\frac{\partial (AS)}{\partial t} \approx 0 = k_1(S)C_g - r \quad (2-12)$$

The system can now be described^[4] by the single differential equation

$$\frac{A\rho C_p}{P} \frac{dT}{dt} = h(T_g - T) + (-\Delta H)k_c C_g \quad (2-13)$$

Following assumption 3) above, each variable in the gas stream will be expressed as the sum of a time averaged value and a fluctuating component. That is:

$$\begin{aligned} T_g &= \langle T_g \rangle + T'_g \\ C_g &= \langle C_g \rangle + C'_g \\ h &= \langle h \rangle + h' \\ k_c &= \langle k_c \rangle + k'_c \end{aligned} \quad (2-14)$$

Also, it will be assumed that the temperature of the wire can be expressed as

$$T = \langle T \rangle + T' \quad (2-15)$$

When N_{Le} is close to unity, Edwards^[4] has shown that substitution of Eqs. (2-14) and (2-15) into (2-13) yields

$$\tau_o \frac{d\theta'_w}{dt} + \theta'_w = \theta'_g + C' \quad (2-16)$$

where

$$\tau_o = \frac{A\rho C_p}{P\langle h \rangle}$$

$$\theta'_w = T' / \langle \Delta T_{ad}^* \rangle$$

$$\theta'_g = T'_g / \langle \Delta T_{ad}^* \rangle$$

$$C' = C'_g / \langle C_g \rangle$$

Most of the experiments reported in this work are for the oxidation of hydrogen in excess air. The values in TABLE 2.1 show that for this reaction $N_{Le} \neq 1$ and therefore Equation (2-16) does not describe the system exactly.

Nevertheless, as will be shown in Appendix III, the corrections that arise are small (about 4%) and Eq. (2-16) still will be assumed to describe the phenomenon taking place on the catalytic wire.

C. Electrically Heated Wires

1) Temperature distribution

When a wire of finite length is heated electrically in a stream of uniform temperature, the steady-state energy balance is given by

$$k_w A \frac{d^2 T_w}{dx^2} - hP(T_w - T_g) + JI^2 R(T_w) = 0 \quad (2-17)$$

Usually the temperature dependence of the electric resistance of the wire gives a first order effect^[6]. Hence

$$R(T_w) = R(T_g) + \beta R_o (T_w - T_g) \quad (2-18)$$

and Eq. (2-17) becomes

$$k_w A \frac{d^2 T_w}{dx^2} - [hP - JI^2 R_o \beta] (T_w - T_g) + JI^2 R(T_g) = 0 \quad (2-19)$$

Edwards^[4] defined an average heat transfer coefficient (\bar{h}) and a fractional heat loss due to radiation and conduction (η) so that Eq. (2-19) could be rewritten as

$$\frac{d^2 T_w}{ds^2} - \lambda^2 (T_w - T_g) + \phi = 0 \quad (2-20)$$

where

$$s = 2(x - x_c) / l_w$$

$$\lambda^2 = \left(\frac{\ell_w}{d_w}\right)^2 \left[\frac{JI^2 R_o \beta [R(T_g) - \eta R(\bar{T}_w)]}{k_w \pi [R(\bar{T}_w) - R(T_g)]} \right] \quad (2-21)$$

$$\phi = \frac{JI^2 R(T_g)}{k_w \pi} \left(\frac{\ell_w}{d_w}\right)^2 \quad (2-22)$$

Subject to boundary conditions

$$T_w = T_g \quad \text{at } s = -1, 1 \quad (2-23)$$

The time averaged temperature distribution along the wire, obtained by solving Eqs. (2-20) and (2-23) is

$$\frac{\langle T_w \rangle - T_g}{\bar{T}_w - T_g} = \frac{1 - \cosh(\lambda s)/\cosh \lambda}{1 - \tanh(\lambda)/\lambda} \quad (2-24)$$

Knowing this temperature profile, the fractional conduction and radiation losses can be defined as^[4]

$$\eta_k = \left(\frac{d_w}{\ell_w}\right)^2 \frac{\pi k_w \lambda \tanh \lambda (\bar{T}_w - T_g)}{JI^2 R(\bar{T}_w) (1 - \tanh \lambda/\lambda)} \quad (2-25)$$

$$\eta_r = \frac{P \sigma}{JI^2 R(\bar{T}_w)} \int_0^1 \epsilon [\langle T_w \rangle^4 - T_g^4] ds \quad (2-26)$$

respectively.

Since

$$\eta = \eta_k + \eta_r \quad (2-27)$$

an iterative solution of Eq. (2-21), (2-25), (2-26) and (2-27) will give the appropriate values of λ and η for each case.

For reasons which will be explained later, in this study we are more interested in the temperature at the center of the wire. This is given by

$$\frac{\langle T_c \rangle - T_g}{\bar{T}_w - T_g} = \frac{\lambda \cosh \lambda - \lambda}{\lambda \cosh \lambda - \sinh \lambda} \quad (2-28)$$

Both Eqs. (2-24) and (2-28) have been experimentally verified^[7].

2) Constant temperature measurement of velocity fluctuations

When the length to diameter ratio for a given wire is larger than 200, Equation (2-17) can be simplified to

$$hP(T_g - T_w) + JI^2R(T_w) = 0 \quad (2-30)$$

If it assumed that h and I can be expressed as

$$\begin{aligned} h &= \langle h \rangle + h' \\ I &= \langle I \rangle + i \end{aligned} \quad (2-31)$$

Eq. (2-30) takes the form

$$1 + \frac{h'}{\langle h \rangle} = \frac{JR(T_w) \langle I \rangle^2}{\langle h \rangle P(T_w - T_g)} \left(1 + \frac{2i}{\langle I \rangle} + \frac{i^2}{\langle I \rangle^2} \right) \quad (2-32)$$

The following empirical correlation describes the heat transfer from a cylinder to a gas flowing perpendicular to its axis^[8].

$$N_{Nu} = B_1 + B_2 (N_{Re})^n \quad (2-33)$$

or

$$h = A + B u^n \quad (2-34)$$

Introducing fluctuating quantities for the velocity (u) and heat transfer coefficient (h), Eq. (2-34) becomes

$$\langle h \rangle \left(1 + \frac{h'}{\langle h \rangle} \right) = A + B \langle u \rangle^n \left(1 + \frac{u'}{\langle u \rangle} \right)^n \quad (2-35)$$

If the fluctuating quantities are much smaller than their time averaged values, from (2-34)

$$\langle h \rangle = A + B \langle u \rangle^n \quad (2-36)$$

Neglecting terms higher than first order Eq. (2-35) yields

$$\langle h \rangle \frac{h'}{\langle h \rangle} = n B \langle u \rangle^n \frac{u'}{\langle u \rangle} \quad (2-37)$$

or

$$\frac{h'}{\langle h \rangle} = \frac{B \langle u \rangle^n}{A + B \langle u \rangle^n} n \frac{u'}{\langle u \rangle} \quad (2-38)$$

Similarly, neglecting second order terms and noting that

$$\frac{J R(T_w) \langle I \rangle^2}{\langle h \rangle P(T_w - T_g)} = 1 \quad (2-39)$$

Eq. (2-32) becomes

$$\frac{h'}{\langle h \rangle} = \frac{2i}{\langle I \rangle} \quad (2-40)$$

Substitution of Eq. (2-38) into Eq. (2-40) and noting that for constant temperature operation $e/i = \langle R \rangle = \text{constant}$, yields

$$\frac{2e}{\langle E \rangle} = n f \frac{u'}{\langle u \rangle} \quad (2-41)$$

where

$$f = \frac{B \langle u \rangle^n}{A + B \langle u \rangle^n} \quad (2-42)$$

Squaring Eq. (2-41), time averaging, and taking the square root, gives

$$\frac{2e_{\text{rms}}}{\langle E \rangle} = n f \frac{u'_{\text{rms}}}{\langle u \rangle} \quad (2-43)$$

Eq. (2-43) relates the turbulence intensity in the gas to the rms value of the fluctuating voltage. It applies only to constant temperature operation and its usefulness depends on a good knowledge of the constants in Eq. (2-34).

3) Reaction and constant temperature measurement of concentration fluctuations

If in addition to electrical heating, the wire is sustaining a chemical reaction on its surface, the mass and energy balances will be

$$\frac{d(AS)}{dt} = k_1 C_g (S) - r \quad (2-1)$$

$$\frac{A\rho C_p}{P} \frac{dT_w}{dt} = h(T_g - T_w) + (-\Delta H)r + \frac{JI^2 R_w}{P\ell_w} \quad (2-44)$$

In deriving Eq. (2-44) it has been assumed that the wire length to diameter ratio is at least 200:1.

If the reaction is mass transfer controlled, $(AS/L) \ll 1$. Furthermore, the wire temperature can be controlled by a constant temperature anemometer so that dT_w/dt vanishes.

Then, Eq. (2-44) becomes

$$0 = h(T_g - T_w) + (-\Delta H)k_c C_g + \frac{JI^2 R_w}{P\ell_w} \quad (2-45)$$

The time average of Eq. (2-45) can be approximated by

$$\langle h \rangle (T_w - T_g) = (-\Delta H) \langle k_c \rangle \langle C_g \rangle + \frac{J \langle I \rangle^2 R_w}{P \ell_w} \quad (2-46)$$

In the limit, when the electric current is completely cut off by the feedback circuit of the anemometer

$$\langle h \rangle (T_w^* - T_g) = (-\Delta H) \langle k_c \rangle \langle C_g \rangle \quad (2-47)$$

Subtracting Eq. (2-47) from Eq. (2-46) yields

$$\langle h \rangle (T_w - T_w^*) = J \langle I \rangle^2 R_w / P \ell_w \quad (2-48)$$

and dividing Eq. (2-45) by Eq. (2-47)

$$\frac{h}{\langle h \rangle} \left(\frac{T_w - T_g}{T_w^* - T_g} \right) = \frac{k_c}{\langle k_c \rangle} \frac{C_g}{\langle C_g \rangle} + \frac{J I^2 R_w}{P \ell_w \langle h \rangle (T_w^* - T_g)} \quad (2-49)$$

Introducing fluctuating quantities in (2-49) and rearranging gives

$$\left(1 + \frac{h'}{\langle h \rangle} \right) \left(\frac{T_w - T_g}{T_w^* - T_g} \right) = \left(1 + \frac{k'_c}{\langle k_c \rangle} \right) \left(1 + \frac{C'_g}{\langle C_g \rangle} \right) + \frac{J I^2 R_w}{P \ell_w \langle h \rangle (T_w^* - T_g)} \quad (2-50)$$

The analogy for $N_{Le} = 1$.

$$N_{Nu} = N_{Sh} = B_1 + B_2 (N_{Re})^n \quad (2-51)$$

can be used to show that

$$\frac{h'}{\langle h \rangle} = \frac{k'_c}{\langle k_c \rangle} \quad (2-52)$$

so that Eq. (2-50) becomes after neglecting second order terms

$$\left(\frac{T_w - T_w^*}{T_w - T_g} \right) \left(1 + \frac{h'}{\langle h \rangle} \right) = \frac{C'_g}{\langle C_g \rangle} + \frac{J \langle I \rangle^2 R_w}{\langle h \rangle P \ell_w (T_w^* - T_g)} \left(1 + \frac{2i}{\langle I \rangle} \right) \quad (2-53)$$

Eq. (2-53) can be further simplified by defining

$$m \equiv \frac{T_w^* - T_g}{T_w - T_w^*} \quad (2-54)$$

and noting that, from Eq. (2-48),

$$\frac{J \langle I \rangle^2 R_w}{\langle h \rangle P \ell_w (T_w - T_w^*)} = 1$$

Hence

$$\frac{h'}{\langle h \rangle} = m \frac{C'_g}{\langle C_g \rangle} + 2 \frac{i}{\langle I \rangle} \quad (2-55)$$

In the absence of concentration fluctuations, Eq. (2-55) reduces to Eq. (2-40) previously derived for the non-reaction case.

Substitution of (2-38) into (2-55) squaring and time averaging yields

$$\langle \left(\frac{2e}{\langle E \rangle} \right)^2 \rangle = \langle \left(n f \frac{u'}{\langle u \rangle} \right)^2 \rangle - 2mn \left\langle \left(\frac{fu'}{\langle u \rangle} \frac{C'_g}{\langle C_g \rangle} \right) \right\rangle + m^2 \langle \left(\frac{C'_g}{\langle C_g \rangle} \right)^2 \rangle \quad (2-56)$$

It follows that by operating the system at three different values of m , one can compute - in principle - the turbulent intensity, the intensity of the concentration fluctuations and the velocity-concentration cross correlation, R_{uc} [4]. The derivation of Eq. (2-56) for cases in which N_{Le} is different from unity is presented in Appendix III.

D. Random Stationary Processes

In this section some properties of random processes of interest for this particular work are described. A more detailed presentation can be found in Reference [9].

The auto-correlation of a random stationary process $\{y_k(t)\}$ is defined as

$$R_{YY}(\tau) = \int_{-\infty}^{\infty} \int_{-\infty}^{\infty} y_1 y_2 p(y_1, y_2) dy_1 dy_2 \quad (2-57)$$

where $p(y_1, y_2)$ is the joint probability density function associated with the pair of random variables $y_1 = y_k(t)$ and $y_2 = y_k(t + \tau)$.

The mean value of y satisfies the relation

$$\langle y \rangle = \sqrt{R_{YY}(\infty)} \quad (2-58)$$

The power spectrum of a signal $y_k(t)$ is the Fourier transform of its autocorrelation

$$S_Y(f) = \int_{-\infty}^{\infty} R_{YY}(\tau) e^{-j2\pi f\tau} d\tau \quad (2-59)$$

Using symmetry properties of stationary correlation functions, Eq. (2-59) can be simplified to

$$S_Y(f) = \int_{-\infty}^{\infty} R_{YY}(\tau) \cos(2\pi f\tau) d\tau \quad (2-60)$$

In practice one is interested in the one-sided power spectral density function, $G_Y(f)$, defined as

$$G_Y(f) = \begin{cases} 2S_Y(f) & 0 \leq f < \infty \\ 0 & \text{otherwise} \end{cases} \quad (2-61)$$

or, in terms of $R_{YY}(\tau)$

$$G_Y(f) = 4 \int_0^{\infty} R_{YY}(\tau) \cos(2\pi f\tau) d\tau \quad (2-62)$$

$0 \leq f < \infty$

The root mean square (rms) and the half power frequency ($f_{1/2}$) are defined as

$$(y_{\text{rms}})^2 = \langle y^2 \rangle = \int_0^{\infty} G_Y(f) df = R_{YY}(0) \quad (2-63)$$

$$\int_0^{f_{1/2}} G_Y(f) df = \int_{f_{1/2}}^{\infty} G_Y(f) df = \frac{1}{2} \langle y^2 \rangle \quad (2-64)$$

The Fourier transform, $H(f)$, of the response of a first order system to an input $h(t)$, is defined^[10] as the system's transfer function

$$H(f) = \int_{-\infty}^{\infty} h(t) e^{-j2\pi ft} dt \quad (2-65)$$

If the platinum wires behave as first order systems the square of the absolute value of the transfer function is given by^[9]

$$|H(f)|^2 = \frac{K}{1 + (2\pi\tau_w f)^2} \quad (2-66)$$

where τ_w is the characteristic time constant of the wire.

Hence, for a first order system, the relation between the input disturbance, G_x , and output signal, G_y , will be:

$$G_Y(f) = |H(f)|^2 G_X(f) \quad (2-67)$$

E. Turbulent Flow Properties

Some properties of turbulent flow are defined below. A more thorough discussion of this subject can be found in Reference [6].

For the case of homogeneous isotropic turbulence, the longitudinal correlation coefficient $f(r)$ and the Eulerian time correlation $R_E(t)$ are defined as

$$f(r) = \frac{\langle (u'_r)_A (u'_r)_B \rangle}{\langle u'^2 \rangle} \quad (2-68)$$

$$R_E(t) = \frac{\langle u'(\tau) u'(\tau - t) \rangle}{\langle u'^2 \rangle} \quad (2-69)$$

where u' is the local fluctuation of the velocity. Subscripts A and B refer to two points along the flow axis separated by a distance r .

Other parameters of importance are the integral length scale Λ_f and the Eulerian time scale τ_E which are defined as

$$\Lambda_f = \int_0^{\infty} f(r) dr \quad (2-70)$$

$$\tau_E = \int_0^{\infty} R_E(t) dt \quad (2-71)$$

If the flow field has uniform mean velocity $\langle U \rangle$ in the x_1 direction and $u_1'/\langle U \rangle \ll 1$, a simple relation between τ_E and Λ_f exists

$$\Lambda_f = \langle U \rangle \tau_E \quad (2-72)$$

$$f(x_1) = R_E(t) \quad (2-73)$$

A good approximation for the Eulerian time correlation is^[6]

$$R_E(t) = \exp(-t/\tau_E) \quad (2-74)$$

However, as pointed out by Hinze^[6] this expression can not be exact since it is not parabolic in its vertex and is positive for all values of its argument.

The one dimensional spectral density function of turbulence $E_1(f)$ is defined as^[6]

$$E_1(f) = \frac{4\langle u_1'^2 \rangle}{\langle U \rangle} \int_0^\infty f(x_1) \cos \frac{2\pi f x_1}{\langle U \rangle} dx_1 \quad (2-75)$$

Substitution of Eq. (2-72), (2-73) and (2-74) into Eq. (2-75) gives

$$\frac{E_1(f)}{4\langle u_1'^2 \rangle \tau_E} = \frac{1}{1 + (2\pi f \tau_E)^2} \quad (2-76)$$

Application of Eq. (2-64) to (2-76) yields

$$\tau_E = 1/(2\pi f_{1/2}) \quad (2-77)$$

which can be substituted back into Eqs. (2-74) and (2-76) to obtain

$$R_E(t) = \exp(-2\pi f_{1/2} t) \quad (2-78)$$

$$\frac{E_1(f)}{4\langle u_1^2 \rangle \tau_E} = \frac{1}{1 + (f/f_{1/2})^2} \quad (2-79)$$

This is a good approximation of $E_1(f)$ for low frequencies.

F. Spectra Relations for Reacting Wires

The pseudo-steady state model [Section B] predicted that flickering exists only when concentration and/or temperature fluctuations are present in the stream of reactants.

If the fluctuations of the gas temperature are negligible Fourier transformation of Eq. (2-16) yields

$$G_{\theta'}(f) = \frac{G_{C'}(f)}{[1 + (2\pi f \tau_0)^2]} \quad (2-80)$$

where $G_{C'}(f)$ is the power spectrum of concentration fluctuations,

The spectral density function of concentration fluctuations should be similar to that of velocity fluctuations in a turbulent flow field (Eq. 2-76). Therefore, a useful approximation would be

$$\frac{G_{C'}(f)}{4\langle C'^2 \rangle \tau_c} = \frac{1}{1 + (2\pi f \tau_c)^2} \quad (2-81)$$

where τ_c is the Eulerian concentration time scale.

Substitution of Eq. (2-81) into (2-80) integration over all possible frequencies and application of Eq. (2-63) yields

$$\frac{\langle T'^2 \rangle}{\langle T - T_g \rangle^2} = \frac{\tau_c \langle C' \rangle^2}{(\tau_c + \tau) \langle C \rangle^2} \quad (2-82)$$

In this way, individual measurements of concentration and temperature fluctuations in the same flow field can be used to test the validity of Eq. (2-82). By doing this at several levels of concentration fluctuations, the main cause of flickering can be determined.

CHAPTER III
EXPERIMENTAL SYSTEM

A. General Description

An overall view of the apparatus used is shown schematically in Figure (3.1). The mixture of either hydrogen or ammonia in air was directed to two wire screens in series with a bundle of tubes at the entrance of the flow channel. This was done to promote a more uniform velocity distribution.

The reactants then passed over a single platinum wire positioned as close as possible to the center line at the downstream end of the channel. The wire was always placed normal to the flow direction. Wires of different diameters and lengths were used. The radiant energy emanating from their surface during the reaction passed through a sapphire window on the top of the channel and was focused on the sensitive portion of the infrared detector. The beam was then mechanically chopped so that AC amplification could be used.

Once the signal was amplified and demodulated, it was passed through a logarithmic amplifier in order to obtain a linear temperature-voltage relationship. Finally, this linearized output was passed through two summers in series before recording or measuring the rms of the fluctuating part of it. Measurements of concentration fluctuations were carried out with non-reacting mixtures of either hydrogen in nitrogen or helium in air flowing

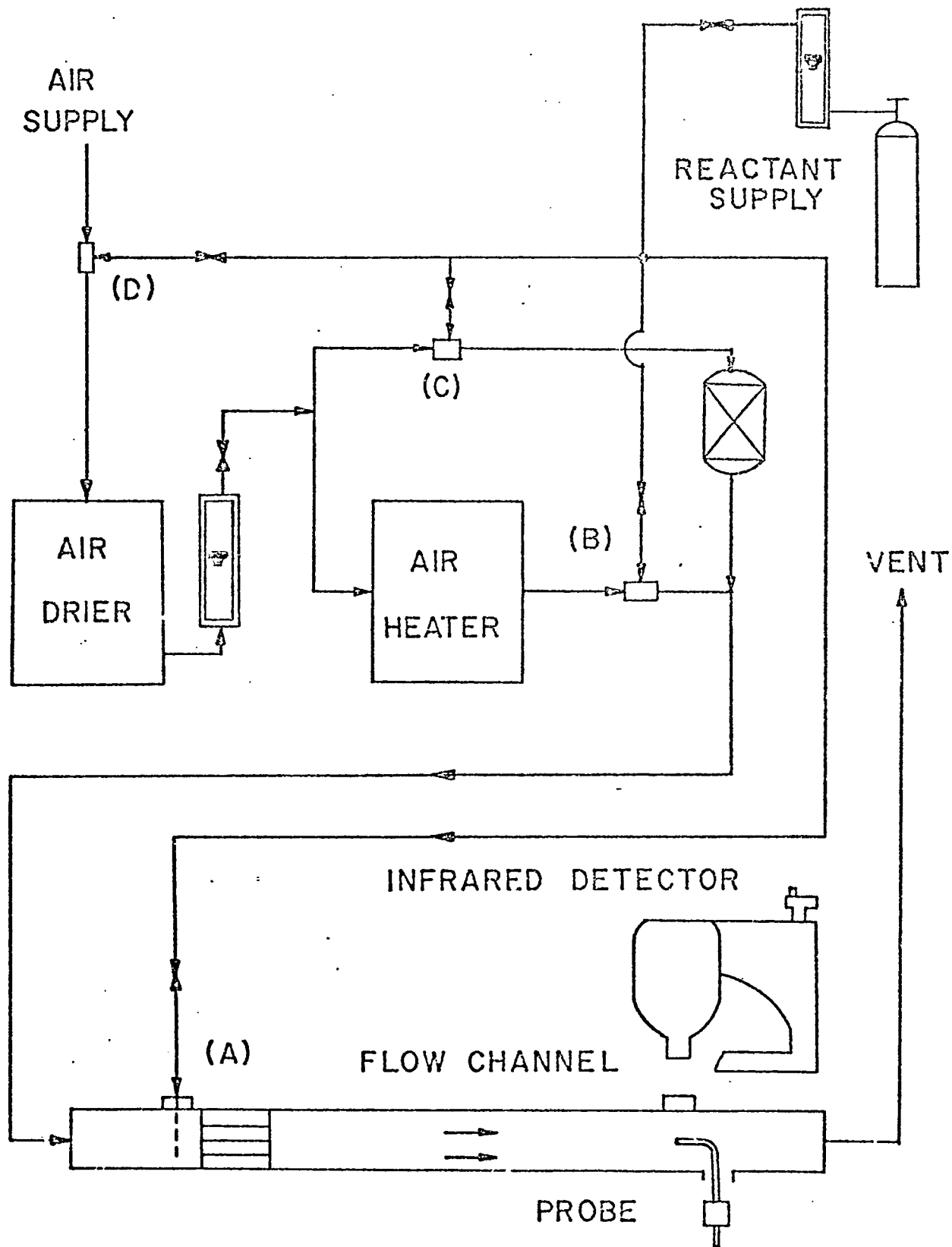


Figure 3.1 - Schematic of overall test assembly

through the channel. The instantaneous fluctuations were detected by an aspirating probe together with a constant temperature anemometer.

The aspirating probe, as well as the hot wire sensor used for turbulence and other constant temperature measurements, were carefully positioned at the location occupied by the platinum wires. This assured results which could be reasonably compared at approximately the same point in space.

B. Flow Channel

The main reactor used is the same as the redesigned flow channel used by Edwards^[4]. It consisted of a 25 x 152 mm cross section chamber 1523 mm long.

The feed gas mixtures entered this channel after passage through a diverging section (127 mm long) with a 12.5 mm diameter opening at its entrance. The entire channel was insulated with a 38 mm thick layer of fiberglass (Figure 3.2).

In order to break up the incoming jet and to provide a uniform velocity distribution, the gas was passed through two 30 mesh stainless steel screens 100 mm apart.

A section packed with 6.3 mm I.D. by 102 mm long stainless steel tubes followed the second screen. Inside these tubes the flow was laminar for the experimental conditions used.

The catalytic wire probe (Figure 3.3) was positioned 700 mm downstream from the exit of the tube bundle. This is equivalent to 16 hydraulic diameters or 56 channel half heights.

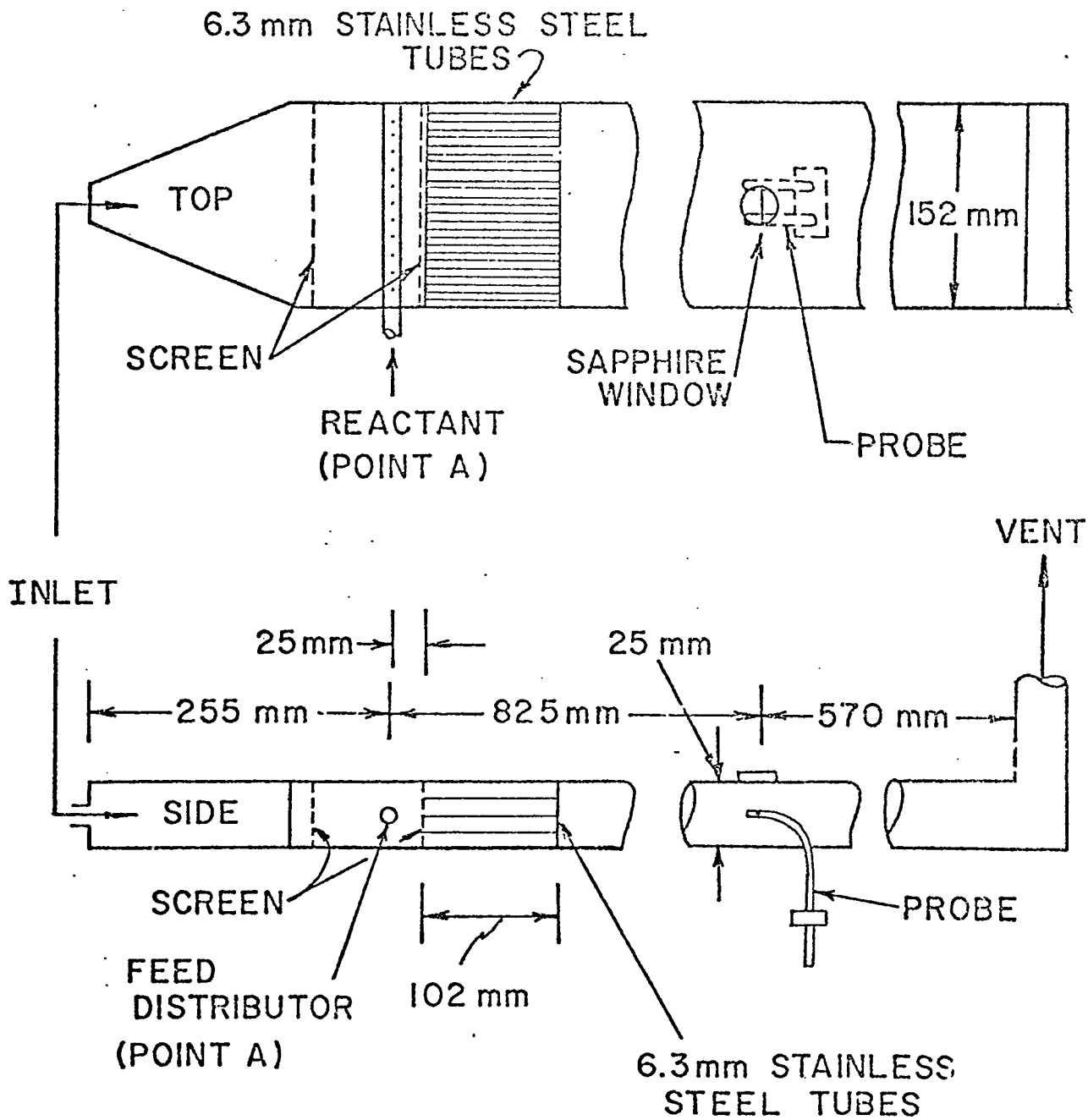


Figure 3.2 - Schematic of the flow channel

On the top of the channel, a 25 mm diameter sapphire window was installed to permit direct viewing of the platinum wire with the infrared unit. On the bottom, the probe opening (12.5 x 50 mm) was sealed with a fiber plate to prevent any gas leakage.

The gas temperature was measured with a mercury in glass thermometer inserted into the channel through a side port near the catalytic wire.

C. Air, Nitrogen and Reactants Supply

In order to obtain an oil-free and pulsation-free discharge, a Gardner-Denver (Model 3CDL5E) compressor was used. This is a rotary screw (3600 RPM) type blower. Air flow rates up to 10855 scm^3/sec at discharge gage pressures up to 0.68 atm were used. Downstream of the compressor the air was measured by a Fisher and Porter Flowmeter (Model 10A3565A) calibrated for 11704 scm^3/sec of air at 1 atm absolute and 21.1°C. Corrections for upstream pressure and temperature were made according to the Equation shown in Appendix I.

Dry grade nitrogen (Union Carbide Co.) was obtained from high pressure cylinders. A warm water bath was used in order to prevent any significant drop in the gas temperature (below T ambient) as it passed through the pressure regulator.

The flow of nitrogen was measured with a Fisher and Porter Flowmeter (serial 6811E1176B) calibrated for 11704 scm^3/sec of air at 1 atm abs and 21.1°C.

The hydrogen and helium flow rates were measured by a Fisher and Porter (Model 10A3565A) tri-flat flowmeter. Calibration curves for the flowrate of these gases (at 0.61 atm constant gage pressure) are shown in Appendix I.

Anhydrous ammonia was supplied from liquified gas cylinders. The flow rate was measured with a Fisher and Porter (Model 10A2735) flowmeter calibrated for $859 \text{ scm}^3/\text{sec}$ of air at 1 atm abs and 21.1°C . A warm water bath was set over the cylinder in order to prevent any undesirable cooling of the gas.

D. Wire Support Probes

The probe assembly used was originally designed to satisfy the following conditions [7]:

- 1) The supporting structure must not catalyze the reaction.
- 2) The wire must be taut at all times to insure proper focusing.
- 3) The resistance of the wire (by itself) must be measurable in order to calibrate the infrared detector output as a function of wire temperature.
- 4) Positioning of the wire in three dimensions must be possible.

The shape of the probes used in this work is shown in Figure (3.3). The wires are inserted through a 0.25 mm hole drilled close to

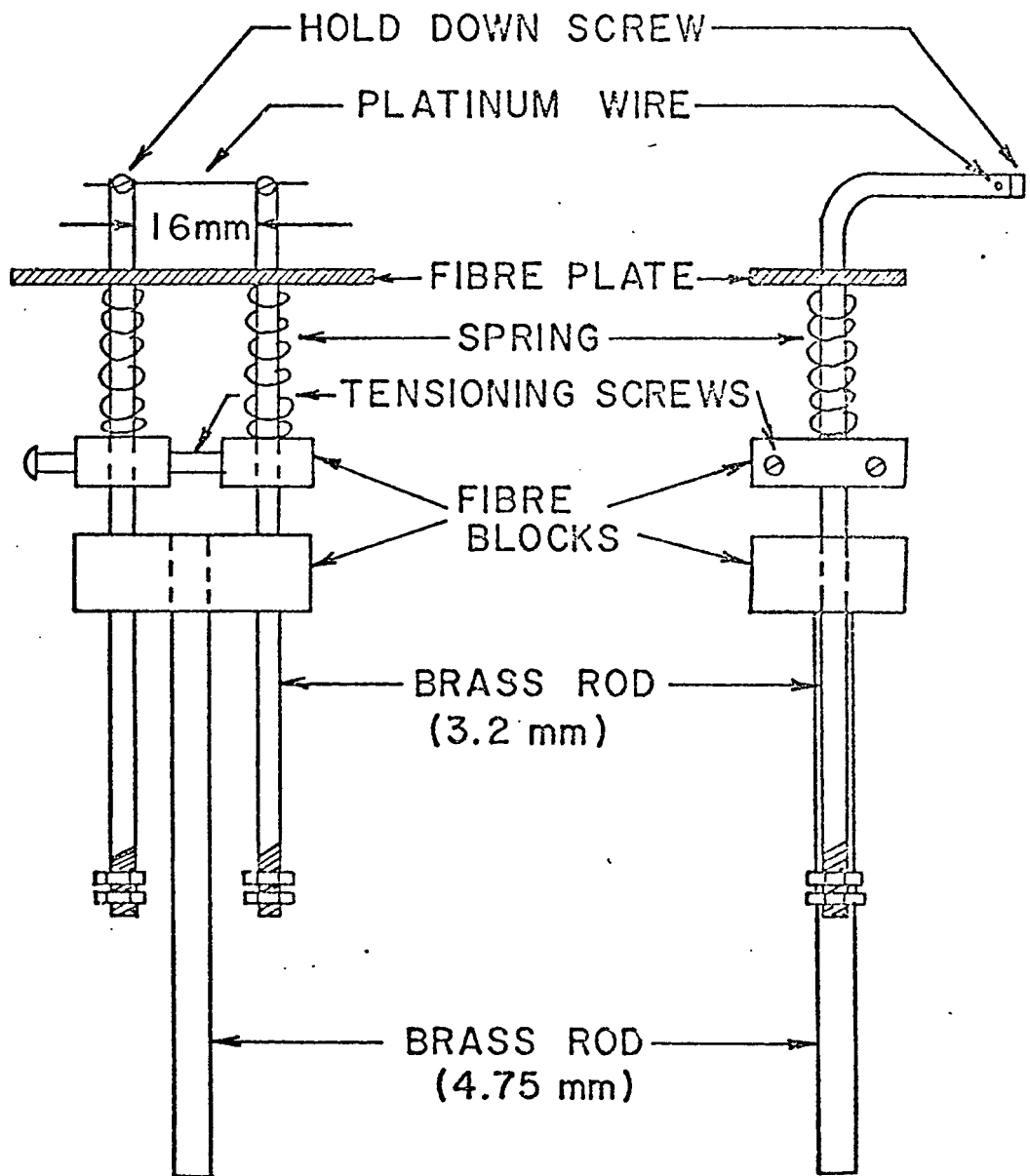


Figure 3.3 - Catalytic wire probe

the tip of the brass rods (3.2 mm diameter), pulled tight, and carefully fastened with the No. 3-48 brass screws.

Two fiber blocks joined by spreading screws served as the tensioning element whenever the wires started to elongate. In this way proper focusing of the wire could be assured throughout the experiment.

The entire wire probe was connected by a 4.75 mm diameter brass rod to a Prior three dimensional microstage. This traverse mechanism has a micrometer scale for each dimension and permits positioning of the wires within ± 0.05 mm.

The probes described so far were used to support platinum wires of 0.012, 0.025, 0.075 and 0.125 mm diameter. These wires were purchased in reels from United Mineral and Chemical Corporation and are reported to be 99.999 percent pure.

For some constant temperature measurements (Chapter V) wires of 0.005 mm diameter were mounted in a special probe (model 1215 V-P2-6) manufactured by Thermo-Systems Inc. The sensing part of these wires was 1.25 mm long with a frequency response of 6.5 KHz.

E. Aspirating Probe

To measure the concentrations fluctuations of hydrogen-nitrogen or helium-air mixtures a Thermo-Systems Inc. (Model 1441A) aspirating probe was used. This probe, shown schematically in Figure (3.4), uses a quartz coated hot film sensor mounted upstream of a sonic nozzle.

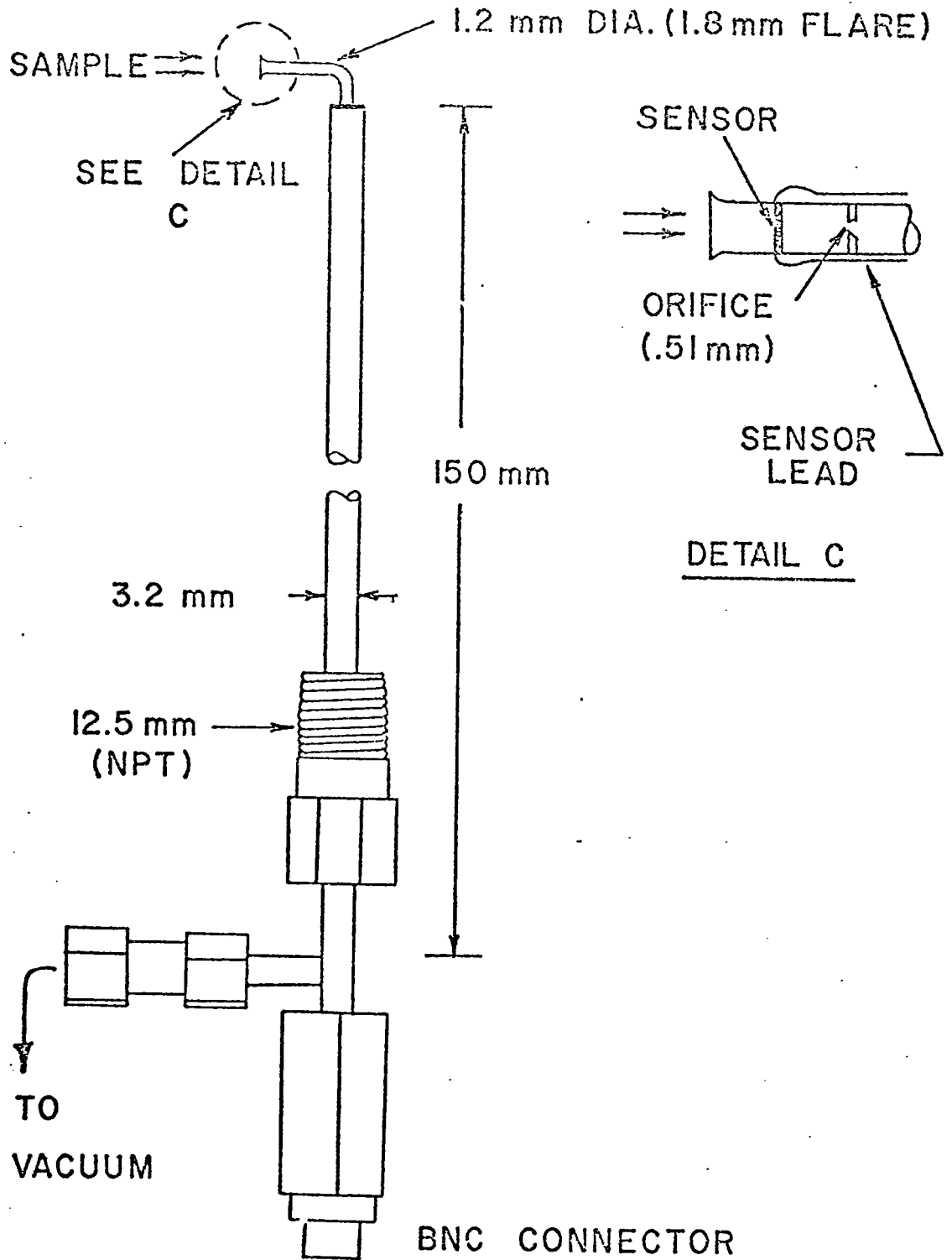


Figure 3.4 - Aspirating probe diagram

The sensor (0.051 mm diameter by 1.0 mm long) detects instantaneous changes in gas temperature, static pressure and velocity, simultaneously measuring fluctuations on the basic properties of the gas as they affect the heat transfer between the sensor and the environment.

The aspirating probe controls the velocity by means of a sonic nozzle. If the temperature is maintained constant it senses gas property changes together with static pressure fluctuations. A small attenuation of the fluctuations may be induced by the probe itself due to non-isokinetic sampling of the gas stream.

When the magnitude of the pressure fluctuations can be neglected (and this is not always the case) the aspirating probe can be used to measure instantaneous composition of a given mixture of gases. To accomplish this, however, the physical properties of the gases (density, viscosity, thermal conductivity) must be widely different.

Connecting the probe to a constant temperature anemometer, the assembly can be used to measure concentration fluctuations in the turbulent stream.

F. Infrared Thermal Microplotter

The instantaneous temperature of the catalytic wires was measured by a Philco Thermal Microplotter (Model 705B). The

unit is shown in Figure (3.5). The radiant energy from the wire first passed through a sapphire window which transmits radiation only in the 1-8 μm range. Then the infrared beam is focused on the sensitive portion of the detector unit, an indium-antimonide cell maintained at 77°K by the liquid nitrogen on the Dewar flash. The radiation beam is mechanically chopped (10 KHz) so that AC amplification may be used.

Detector cell output is fed to the preamplifier and control unit, Figure (3.6), where it is further amplified and demodulated to a 0 - 10 volt DC signal. In this unit, fluctuations with frequency higher than about 320 Hz will be attenuated, since its nominal response time is 0.5 milliseconds.

The demodulated output from the control unit was found to be proportional to the fifth power of the absolute temperature^[7]. Therefore another signal linearization is needed prior to any rms measurement or recording. A Burr-Brown Research Corporation (Model 4007/40) logarithmic amplifier with the property

$$E_{\text{out}} = 10 \log_{10} E_{\text{in}}$$

was used to accomplish this final linearization.

The last two steps for conditioning of the signal before any magnetic tape recordings were made, was to pass it through a DC offset and a band pass-filter. The DC offset unit consists of two operational amplifiers in series (Gain = 1). It permits

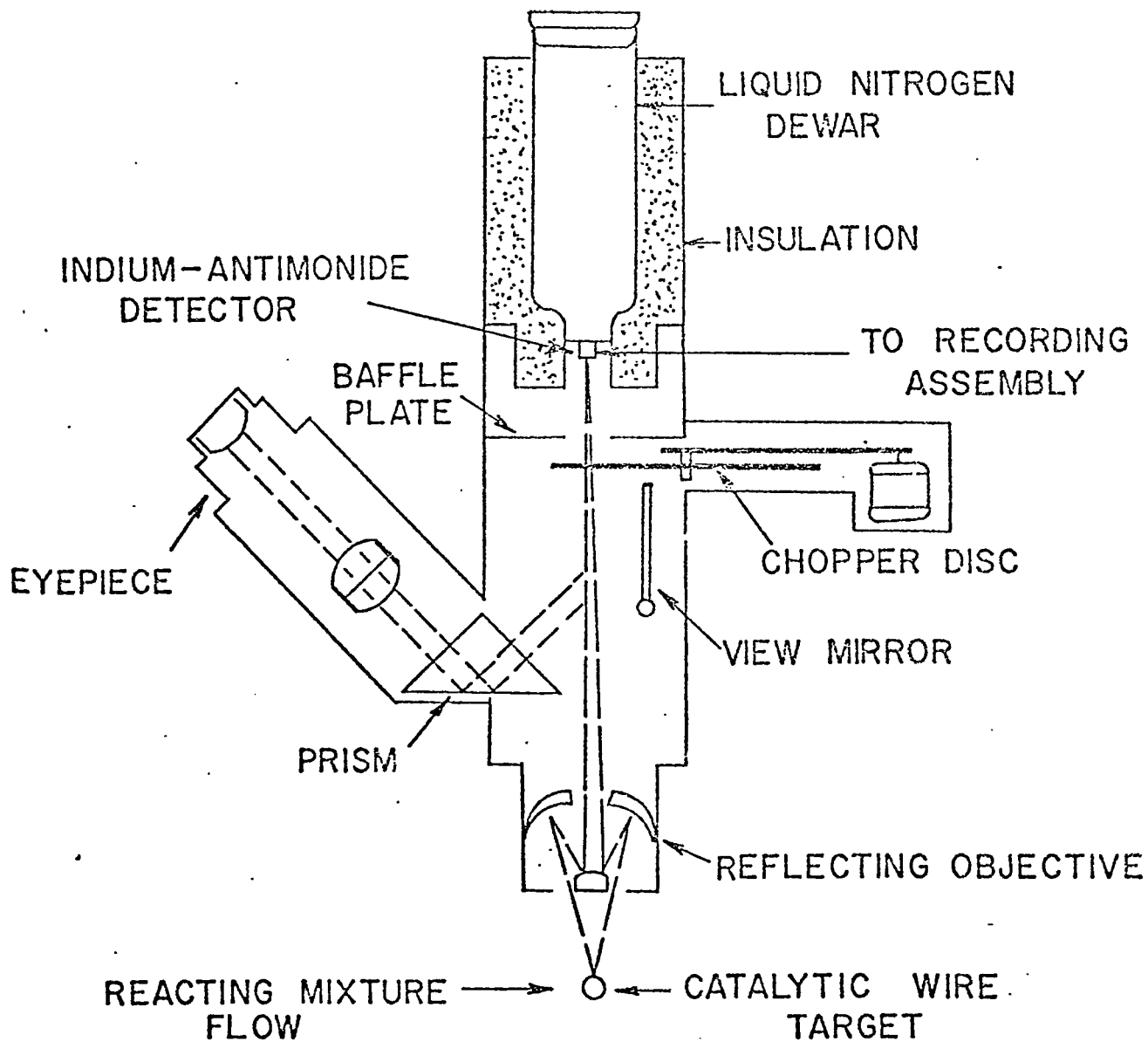


Figure 3.5 - Schematic of infrared thermal microplotter

the measurement of only the fluctuating part of the signal connected at its input.

The Krohn-Hite filter (Model 3750) was used to remove any undesirable high frequency noise coming from the chopper and control unit. It also allowed a broad selection of frequencies of interest which will change as the wire diameter changes [3].

G. Measuring and Recording Equipment

Various apparatus were used to control and measure the electric signals associated with the wires.

Voltages were measured with a Non-Linear Systems, Inc. (Series X-2) digital voltmeter. In the DC mode, readings could be made from 0.001 to 999.9 volts in three ranges. For millivolts measurements, readings could be made from 0.01 mv to 999.9 in two ranges.

The accuracy of this instrument is 0.05% of reading (0.02% of full scale) and the response time .5 seconds.

Wire currents were measured with a Non-Linear Systems, Inc. (Series LX-2) digital multi-function meter, in conjunction with a Leeds and Northrup (CAT. 4385) current shunt. The response time of the digital meter is 0.5 seconds. In the VDC mode it allows readings from 100 μ v to 1000 volts (automatic ranging and polarity selection).

The shunt box displays eight different settings to limit the maximum current from a low .075 amps to a high 15 amps through the circuit. The combined assembly reduced the current measurements to a .07% (full scale) accuracy.

In order to trace visually and to estimate the frequency and peak to peak magnitude of the oscillations, a Hewlett-Packard (Model 1200A) oscilloscope was used. It has bandwidth ranging from DC up to 500 KHZ. Each channel accepts single-ended or differential input signals, either AC or DC coupled. The response time of this Dual Trace oscilloscope is 0.7 microseconds.

Direct measurements of the standard deviation (rms) of the fluctuations were made by a Thermo-Systems Inc. (Model 1060) RMS voltmeter. It permits measurements in random signals with frequencies ranging from 0.1 Hz to 500 Hz. Full scale readings can be made with inputs from 1 millivolt to 300 volts, in 12 ranges.

A time constant switch determines the averaging time of the rms voltmeter and also sets the low pass cutoff of the instrument. It is necessary to wait at least 3 time constants for a reading within 2% of the final value.

In order to assure reasonable accuracy, adjustment to zero was made at the beginning of every experiment. Also, readings were taken only in the upper half of the scales on the panel meter.

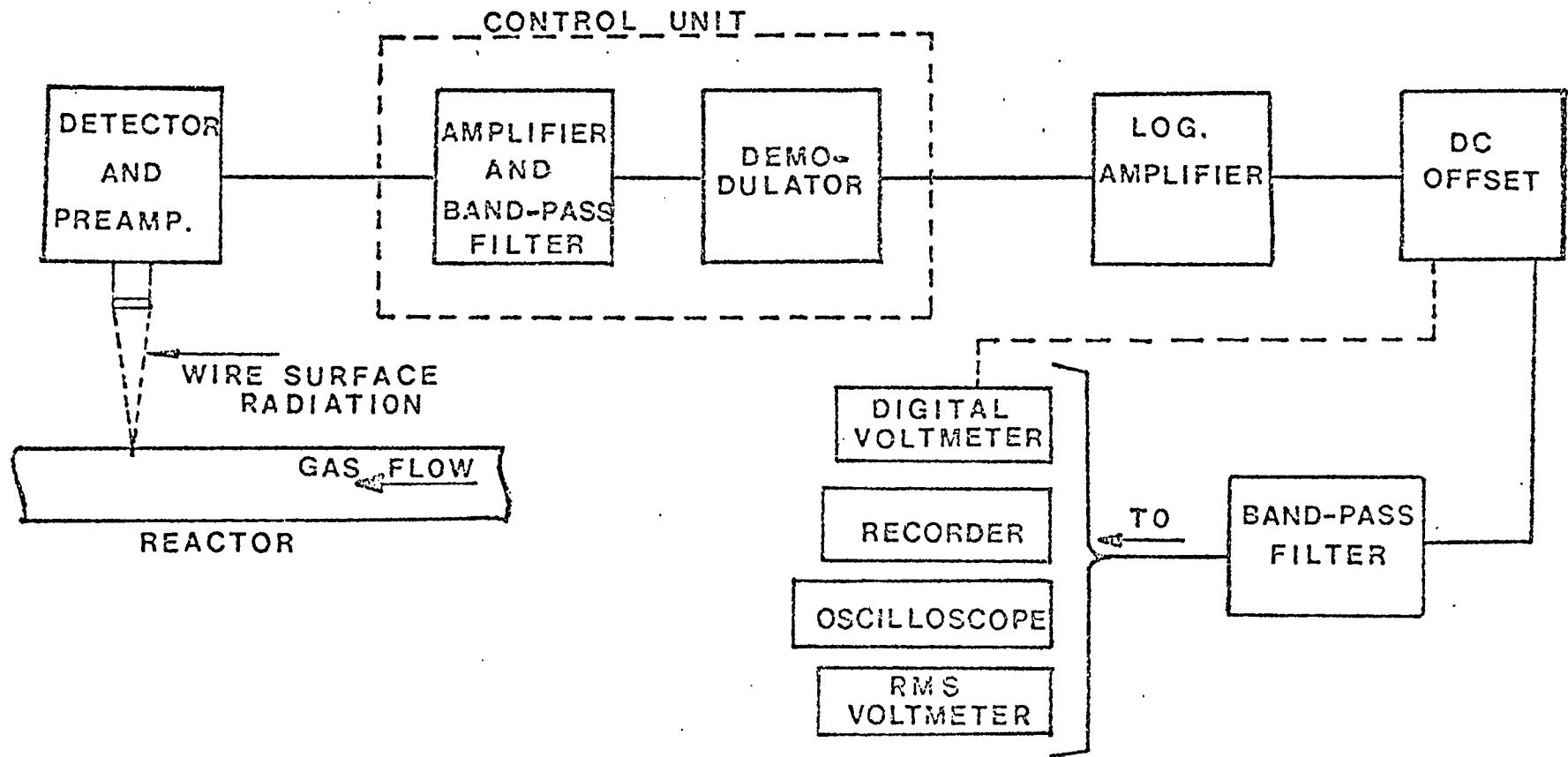


Figure 3.6 - Measuring and recording equipment

This latter procedure was followed as suggested by experimental calibrations^[4].

Magnetic tape recordings of the random signals were obtained using a Hewlett-Packard (Model 3960) Instrumentation Recorder. The recorder has 4 channels and 3 recording speeds (15/16, 3-3/4, & 15 inches per second).

The frequency response is 1250 H_2 at the 3-3/4 ips speed, which was the one used throughout this work. The signal to noise ratio is approximately 48/1 (RMS/RMS). The input level can be varied from 1 to 30 volts (peak-to-peak). The output level is adjustable from 0-5 volts (peak-to-peak). The tape speed accuracy is of the order of 0.2%.

The data recorded on tapes were digitized on a hybrid computer at sampling rates depending on the wire diameter and the frequencies of interest. The digitized data were processed to determine the various statistical properties of the signals.

CHAPTER IV
EXPERIMENTAL TECHNIQUES

In this chapter the general procedure used during reaction experiments is described. Also a description is made of the wire temperature calibration, turbulence and concentration fluctuations measurements.

A. General Procedure

Once the wire had been pulled tight through the probe holes, as described in Chapter III, the upper part of the probe holding the wire was introduced into the reaction channel. The entire assembly was then externally attached to the three dimensional microstage.

By simultaneous manipulation of the infrared detector's microscope and the microstage, the wire was brought into focus and positioned as close as possible to the channel centerline. Then, it was manually adjusted until it was perpendicular to the direction of flow. Before activation, the center of the wire was determined with the aid of the microscope by focusing the crosshairs on each end of the wire. Successive measurements of the horizontal vernier and linear interpolation, permitted the location of the center within 0.05 mm (0.3% of the overall length for most wires).

Activation was started by heating the wire, electrically to a glowing luminosity (approximately 600 - 700°C). After about 30 minutes, the reactant was introduced very slowly into the main stream of air. In most cases, the reactant was fed through point C (Figure 3.1). During this operation, the current was simultaneously reduced in order to prevent excessive sagging but still maintain a glowing wire.

Both reaction on the surface and electrical current through the wire were continued for about another 30 minutes. After this, the surface was active enough to sustain the reaction by itself with no electrical heating.

The mixture of either hydrogen or ammonia in air was allowed to undergo reaction in the wire for an additional period of about 2 hours. No measurements were made during this time except for periodic checks with a 100 mA current to see if the wire was still ignited.

After this treatment the wire's activity was very close to its asymptotic value and, therefore, the emissivity and detector output voltage should not considerably change for a short period of time^[3].

The thermal microplotter is set ready by pouring liquid nitrogen into the Dewar flask to cool the indium-antimonide cell to 77°K. This step must be done very carefully as has been explained elsewhere^[11].

Before any recordings or measurements were made, the stationarity of the process was checked by visual observation of the fluctuating signal on a Hewlett-Packard (Model 1200A) Dual Trace Oscilloscope. If after several minutes no shift in the average output voltage was observed, then recordings and RMS measurements of the linearized detector output were taken.

The data collected on tape were later digitized in a hybrid computer and further processed with a program which uses the fast Fourier transform of Cooley and Tukey^[9]. With the output from this program a detailed analysis can be made of the statistics associated with the fluctuating surface temperature.

B. Wire Temperature Calibration and Measurement

In a previous work, Edwards^[7] used platinum resistivity data taken from Reference [12] and by a least-squares fit obtained the following expression for the resistivity ratio.

$$\frac{R(\bar{T}_w)}{R(0^\circ\text{C})} = 1 + 3.981 \times 10^{-3}\bar{T}_w - 5.849 \times 10^{-7}\bar{T}_w^2 \pm .0002$$

(4-1)

where

\bar{T}_w is in °C.

It becomes evident that when electrically heating a platinum wire, if we can determine the resistance, by solving Eq. (4-1)

we will be able to determine its average temperature. First, of course, $R(0^\circ\text{C})$ must be known.

To determine $R(0^\circ\text{C})$ the voltage drop across the wire is set at several (5 to 7) predetermined values and the current through it is simultaneously measured. The linear (least squares fit) relation between the power input and the resistance of the wire, is extrapolated to zero power in order to estimate $R(\bar{T}_g)$ with an accuracy within 0.5%.

At the same time, measurement of the temperature surrounding the wire can be made with the mercury in glass thermometer placed just upstream of the wire station. By using Eq. (4-1) the resistivity ratio at that temperature, \bar{T}_g , can be obtained. The quotient between the extrapolated value of $R(\bar{T}_g)$ and the calculated resistivity ratio will give the desired value for $R(0^\circ\text{C})$.

After this, the infrared detector output was measured at several wire temperatures while still using electrical heating. Because the infrared unit was focussed on the center of the wire, to complete the calibration, Eq. (2-28) is to be used as the relation between the experimentally measured $\langle\bar{T}_w\rangle$ and the temperature actually being fed to the detector cell, $\langle T_c \rangle$.

A computer program written to perform these calculations, permits a rapid calibration (DCO vs. $\langle T_c \rangle$) before and after any experiment with reaction. For most of the runs, both calibrations were in good agreement, showing that the emissivity of the platinum did not change considerably over a small period of time.

C. Turbulence Measurements

Velocity fluctuations in the channel were measured with a Thermo-Systems Inc. (Model 1010A) constant temperature anemometer. Two different types of sensors were used for separate turbulence experiments. First a TSI 1220G probe with a 60 NQ type sensor was connected to the anemometer. The sensor consisted to a 1000Å^o thick platinum film deposited on a 0.15 mm diameter by 2.0 mm long ceramic cylinder. Its frequency response was 15,000 Hz.

Also measurements were made with a Thermo-Systems Inc. (Model 1215V) probe and a P2 type sensor. This sensor consisted of a brazed mounted platinum wire with a sensing part 1.25 mm long and 0.005 mm in diameter. This is a very sensitive sensor with a frequency response up to 65,000 Hz.

In both cases, the air flow rate through the reactor was varied to cover a wide range of Reynolds numbers. Simultaneous values of bridge voltage and mean velocity were obtained.

Because the sensor is located near the centerline of the channel the mean velocity, $\langle \bar{u} \rangle$, was further used to calculate $\langle u_{\max} \rangle$ past the wire by assuming a power-law type profile for turbulent flow. That is, [13]

$$\frac{\langle \bar{u} \rangle}{\langle u_{\max} \rangle} = \frac{2n^2}{(n+1)(2n+1)} \quad (4.2)$$

with $n = 6$.

The parameters of King's Equation^[14] for hot-wire and hot-film measurements with long cylinders, were then determined for our experimental conditions. To perform this, values of the bridge voltage squared against maximum velocity were fitted using a general purpose non-linear curve fitting subroutine.

The numerical values of K_1, K_2 and n in King's equation

$$E_b^2 = K_1 + K_2 u_{\max}^n \quad (4-3)$$

could be determined within .17% error based on rms deviation of the fit from the experimental points. The details of these calculations are presented in Appendix II.

D. Concentration Fluctuations Measurements

1) Aspirating probe procedure.

The aspirating probe described in Chapter III(Section E) was carefully introduced into the flow channel through the 12.5 x 50 mm bottom opening. With the three dimensional micro-stage, it was positioned near the center line of the chamber and, then, visually oriented until it was parallel facing the gas stream.

The 0.51 mm diameter orifice in the probe tip [Figure 3.5] was connected to a Welch Scientific Co. (Model 1402) vacuum pump, in order to maintain a downstream pressure between 125 - 75 mmHg absolute. This would insure sonic flow through the orifice.

Three surge bottles were connected in series between the suction outlet of the pump and the connecting hose of the probe. In this way most of the undesirable vibrations due to the pump operation were strongly dampened.

However, when the concentration fluctuations in the gas stream are small, the measurements made with the aspirating probe were influenced by strange periodicities and pressure fluctuations. More details of this behavior are discussed in Chapter V.

Calibrations against known composition mixtures and rms voltages determinations were done by connecting the probe to a Thermo-Systems Inc. (Model 1010A) constant temperature anemometer.

2) Constant temperature procedure

According to the theoretical analysis of Chapter II (Section C), flickering can be used as a measure of concentration fluctuations if the pseudo-steady state model is applied at constant temperature operation.

To check this theory a Thermo-Systems Inc. (Model 1215V) probe with a P2 sensor was placed at the channel's wire station. The sensor consisted of a 0.005 mm diameter by 1.25 mm long platinum wire with a frequency response of 65,000 Hz.

The probe was connected to a Thermo-Systems (Model 1010A) constant temperature anemometer and the probe resistance was adjusted for a sensor temperature of about 580 °C.

After 30 minutes, hydrogen (2.5% v) was slowly introduced into the air stream. Point C of Figure 3.1 was used to obtain good mixing of the gases.

The feedback circuit of the anemometer automatically reduced the current in order to maintain a constant wire temperature, when the reaction was initiated. After about 30 minutes, the current was completely shut off and the mixture of 2.5% v hydrogen in air was allowed to react on the wire for an additional period of 2 hours.

After this activation, the hydrogen line was closed and the resistance of the wire with no reaction, R_g , was determined at ambient temperature.

By use of three different overheat ratios, an average value for the turbulence intensity was obtained. Hydrogen was again fed into the system and the resistance of the wire with reaction only, R^* , was determined.

The system was operated at three different values of $\Delta R = R_w - R_w^*$ and the intensity of concentration fluctuations as well as the velocity-concentration cross correlation were calculated. The calculation is described in Chapter V.

CHAPTER V

EXPERIMENTAL RESULTS

A. Preliminary Experiments

Several runs were made to measure the effect of the feeding port (Figure 3.1) on the degree of mixing obtained when helium (3% v) was injected in an air stream. A Thermo-Systems, Inc. (Model 1441A) aspirating probe was used for these measurements.

It was observed that the intensity of concentration fluctuations strongly decreased as the helium feed port was changed from point A to point D (Figure 3.1).

The measurements were repeated injecting hydrogen in a turbulent stream of nitrogen. Air was not used for these experiments to avoid the possibility of a reaction on the quartz coated sensor. However, hydrogen-nitrogen mixtures can be considered very similar to those of hydrogen-air for purposes of concentration fluctuations measurements at the same flow rates.

The results indicated that when the same flow rate and injection point are used, almost a one-to-one relation exists between the helium in air and the hydrogen in nitrogen concentration fluctuation intensity. For $c'_{rms}/\langle c \rangle$ greater than about .05 there is, however, a tendency for the helium fluctuations to be higher than the corresponding hydrogen fluctuations. Some of these results were reported by Edwards [4].

It was also observed during the experiments with helium that by rotating the feed distributor (point A) about its axis, the concentration fluctuation intensity could be made to vary almost by a factor of five. The feed distributor consisted of a 6.4 mm o.d. stainless steel tube with eleven .34 mm diameter holes spaced along its length at 12.5 mm intervals.

This possibility of controlling and measuring the concentration fluctuations over a wide range of intensities, suggested that new experiments could be undertaken to determine if concentration fluctuations were the cause of the flickering observed on reacting wires.

B. Measurements of Hydrogen Concentration Fluctuations

To measure the effect of the injection orientation on the intensity of concentration fluctuations, hydrogen was introduced in the nitrogen stream through the feed distributor located at point A. The open end of the aspirating probe was placed at the catalytic wire station, 825 mm downstream from the feed distributor.

The injection angle was defined as zero degrees for injection in the direction of air flow and positive when measured in the clockwise direction. For example, vertical upward injection corresponds to $\phi = 90^\circ$.

The effect of the angular position of the feed distributor on the concentration fluctuations is shown in Figure (5-1). In

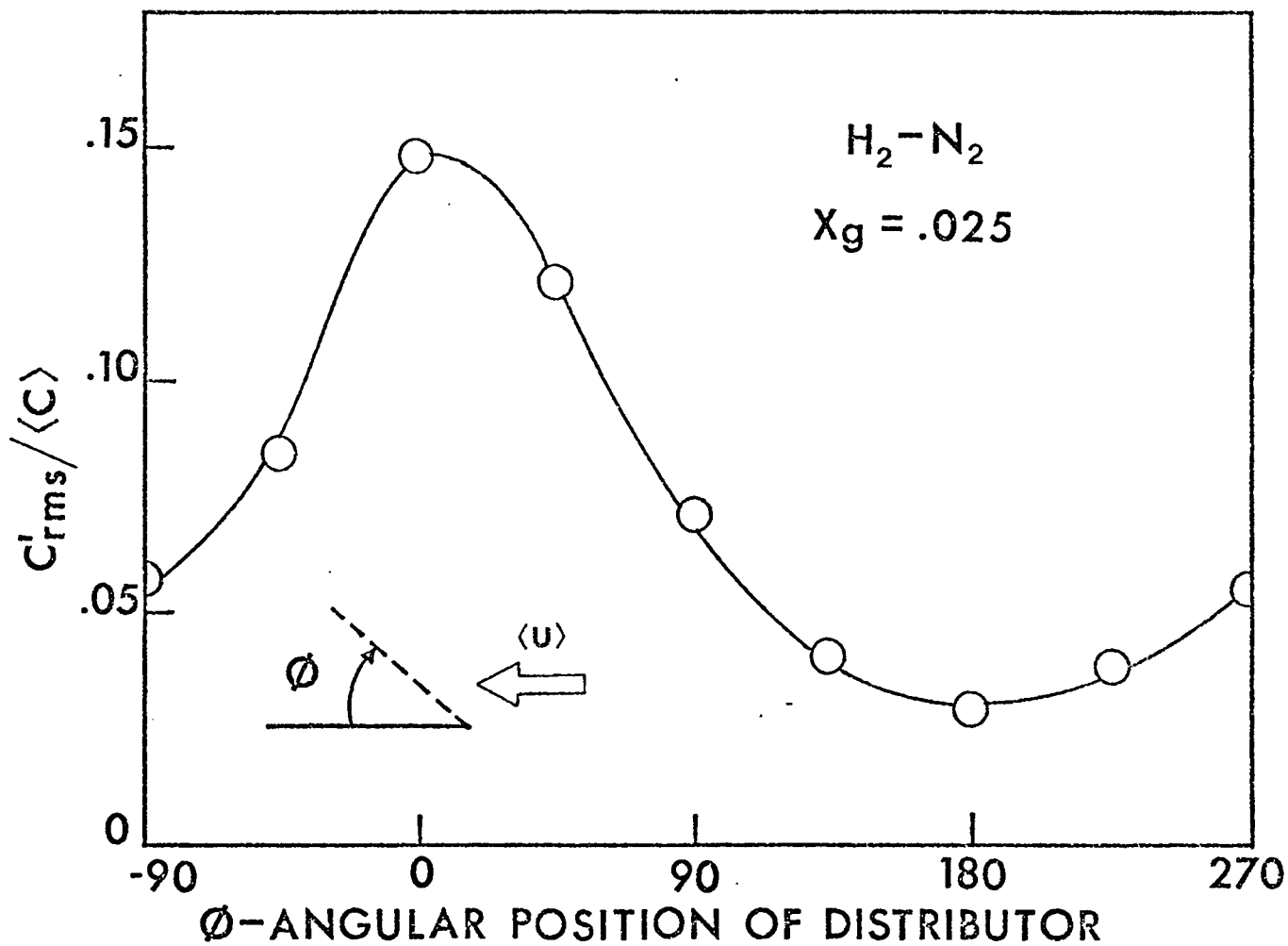


Figure 5.1 - Effect of the injection angle on the concentration fluctuations amplitude ($N_{Re} = 4000$, $T_g = 24$ °C)

these experiments the channel Reynolds number was 4000, the volume fraction of hydrogen $x_g = .025$ and the gas temperature 24°C .

The results show what the intensity of the hydrogen concentration fluctuations at the probe site is strongly dependent on the angle of injection. The magnitude of the fluctuation is seen to decrease by a factor of almost five as the distributor is rotated from 0 degrees to 180 degrees.

Injection of hydrogen into the stream of nitrogen at $\phi = 180^\circ$ appears to give the most uniform concentration distribution at that particular feed point. Downstream injection ($\phi = 0^\circ$), on the other hand, yielded a maximum for the concentration fluctuations intensity.

This type of behavior would be expected since for $\phi = 180^\circ$ the momentum vector of the hydrogen jets is directed opposite to the flow of the nitrogen stream, while for $\phi = 0^\circ$ the momentum vectors are oriented in the same direction. In this latter case, the jets are expected to maintain their identity within the main stream for a longer distance, which yields a mixing of the gases poorer than for the case of $\phi = 180^\circ$. Measurements ($\phi = 0^\circ$) of concentration gradients were made by moving the aspirating probe in the vertical direction. Figure (5.2) shows that a gradient in the time averaged hydrogen concentration exists at the wire station.

The measured mean concentration, 0.021, was less than

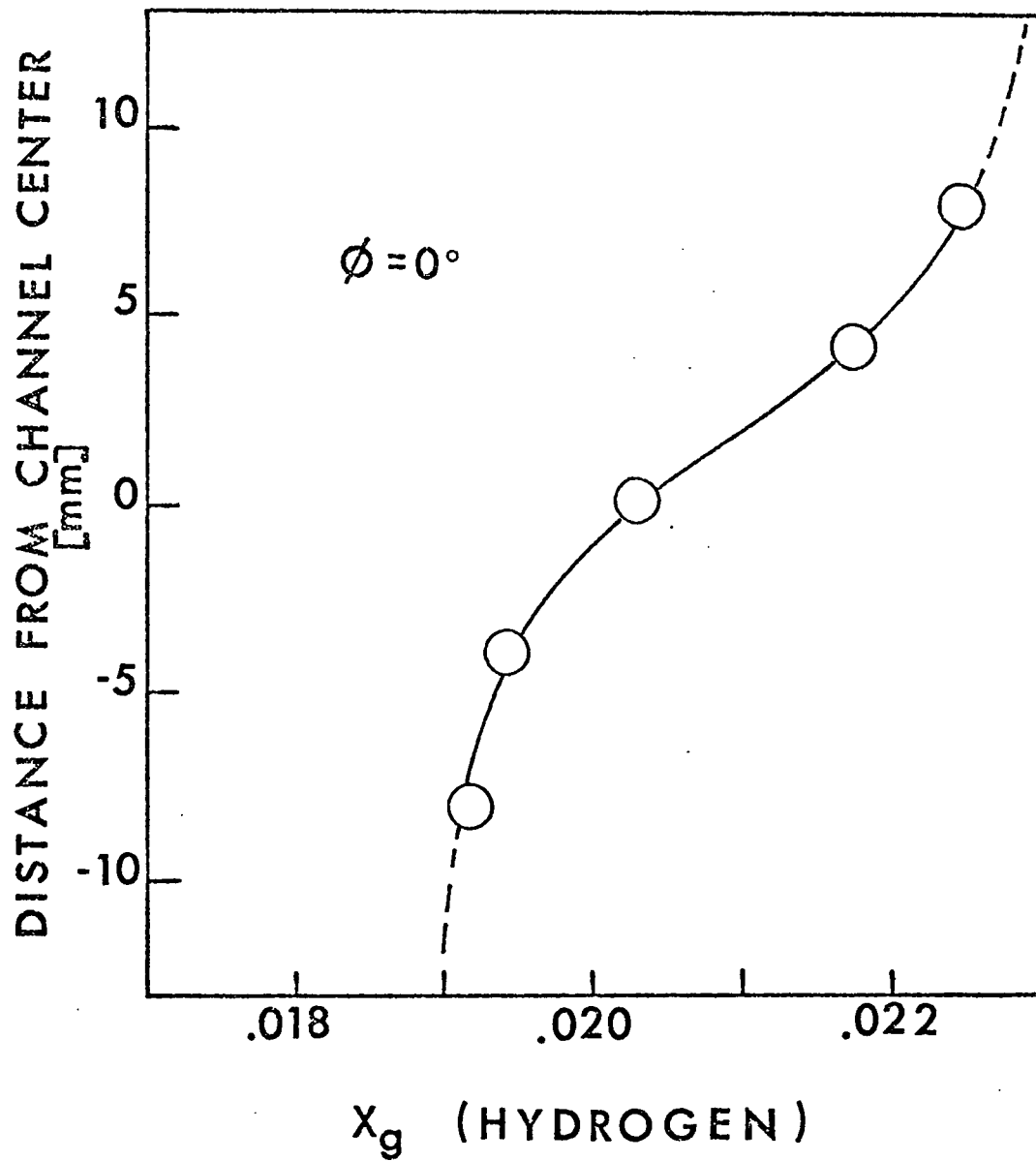


Figure 5.2 - Concentration profile at the wire station ($N_{Re} = 4000$, $x_g = .025$)

0.025 computed from set flow rates. This indicates that horizontal concentration gradients must have existed. No attempt was made, however, to measure the horizontal hydrogen profile.

C. Hydrogen-Air Reaction

A mixture of 2.5%v hydrogen in air was used to study the oxidation of H_2 on the surface of a 0.075 mm diameter platinum wire. The channel Reynolds number was 4000 with $T_g = 24^\circ C$. Point A was used to inject the hydrogen.

The infrared unit was focused at the center of the wire and the average temperature at this point, $\langle T_g \rangle$, plus the fluctuating temperature contribution, T'_{rms} were measured for several angles of injection, ϕ .

Figure 5-3 shows the effect of the injection angle on the temperature fluctuation amplitude. This dependency is very similar to the dependency of the concentration fluctuations on the angle ϕ .

The value of the temperature fluctuations increased from $8.6^\circ C$ (rms) to $33.4^\circ C$ (rms) as the distributor was rotated from 180 degrees to 0 degrees.

D. The Pseudo-Steady State Test

In Chapter II, the assumption that flickering is induced by concentration fluctuations when the capacity term \underline{a} is large, led to the derivation of Eq. (2-83). This equation,

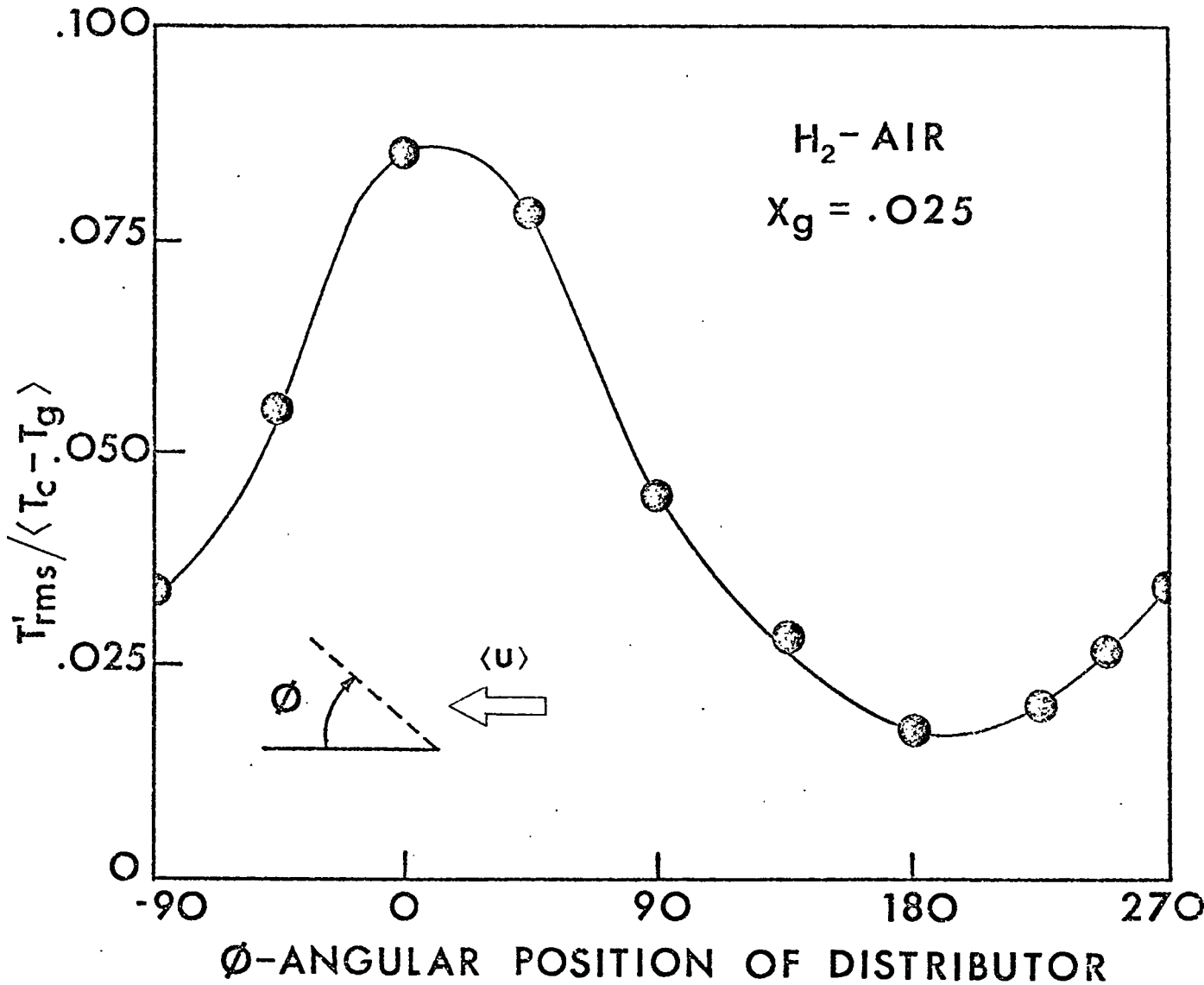


Figure 5.3 - Effect of the injection angle on the temperature fluctuations ($N_{Re} = 4000$, $d_w = .075$ mm, $T_g = 24$ °C)

$$\frac{c'_{rms}}{\langle c \rangle} = \left(\frac{\tau_c + \tau}{\tau_c} \right)^{1/2} \frac{T'_{rms}}{\langle T_c - T_g \rangle} \quad (5-1)$$

can be used to calculate concentration fluctuations from experimental measurements of temperature fluctuations.

These calculations require information about the effect of the injection angle on τ_c . Measurements with the aspirating probe showed that τ_c could vary by as much as 30% when the angle ϕ was changed as described in Figure 5.4

For $x_g = .025$, τ_c varied between .030 and .039 sec. The value of τ for a .075 mm diameter wire was determined by heat transfer experiments as .070 sec.

Table 5.1 presents a comparison of the computed values of $c'_{rms}/\langle c \rangle$ with the experimental measurements of this quantity. The computed results show a very good agreement with the measured values. These results are presented graphically in Figure 5.5b.

TABLE 5.1

Calculated and measured hydrogen fluctuations

Angle ϕ (degrees)	$c'_{rms}/\langle c \rangle$ measured	$c'_{rms}/\langle c \rangle$ computed (Eq. 5-1)
-90	0.057	0.063
-45	0.083	0.097
0	0.146	0.147
+45	0.120	0.137
+90	0.070	0.082
+135	0.040	0.051
+180	0.029	0.028
+225	0.038	0.034

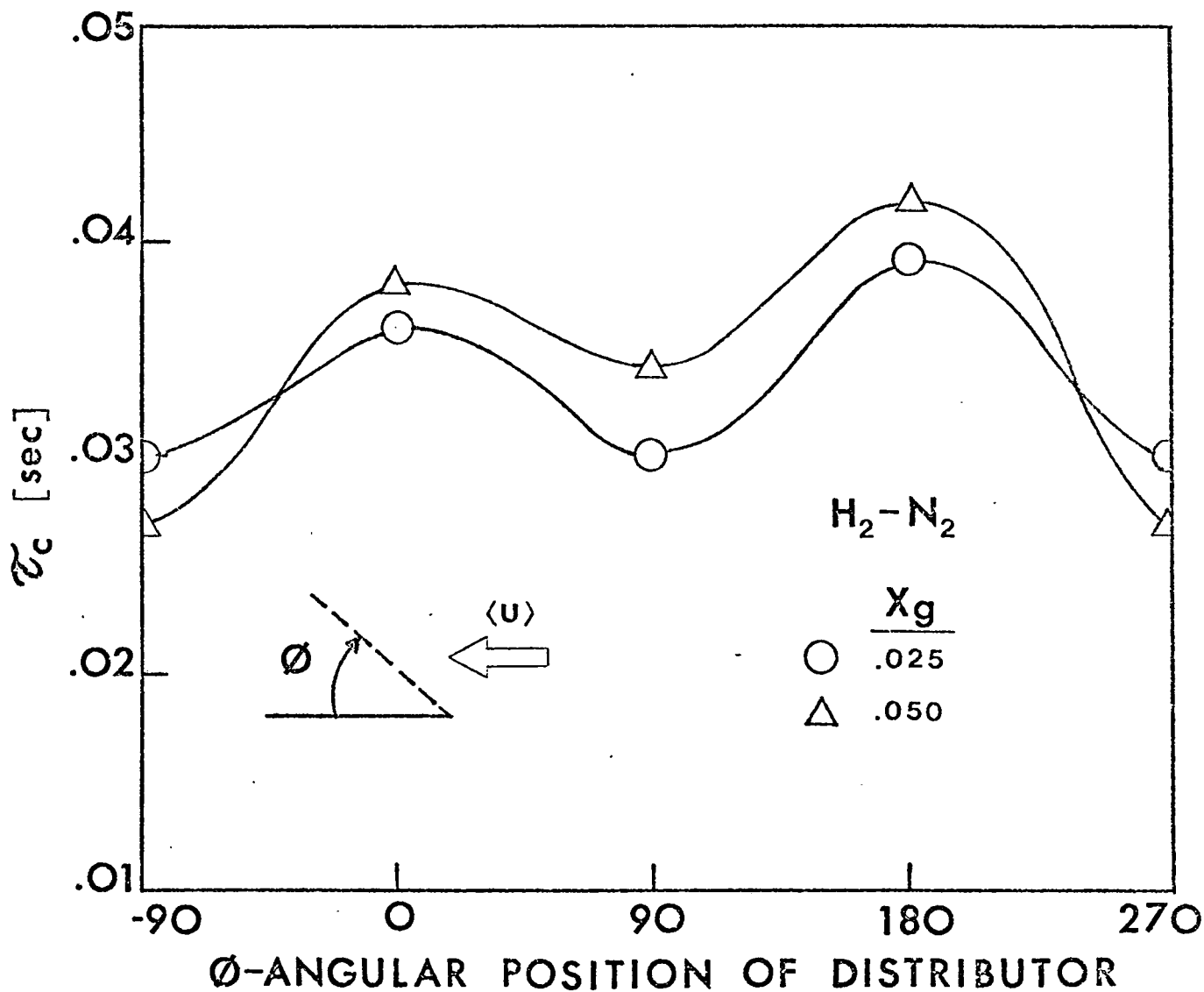


Figure 5.4 - Effect of the angular position of the distributor on τ_c ($N_{Re} = 4000$, $T_g = 24^\circ C$)

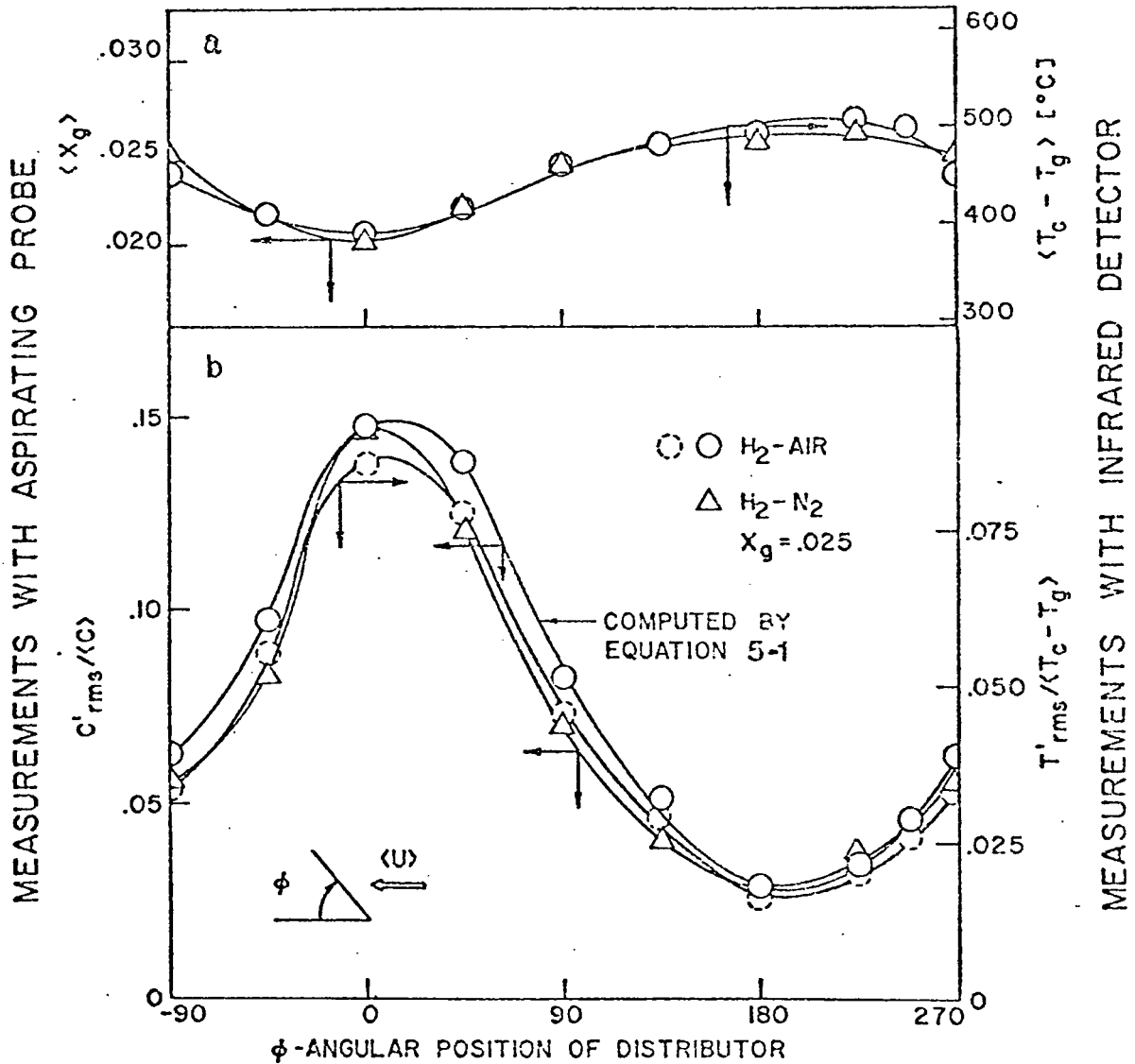


Figure 5.5 - Effect of the injection angle on $\langle X_g \rangle$ and $c'_{rms}/\langle c \rangle$; $T'_{rms}/\langle T_c - T_g \rangle$ for a 0.075 mm wire and on $c'_{rms}/\langle c \rangle$ computed from Eq. (5-1)

When hydrogen was fed at point A, the time averaged concentration $\langle x_g \rangle$ at the wire station depended on the angular position of the feed distributor. As was previously noted, this is due to gradients which develop as the angle ϕ is changed.

In Figure (5-5a), the comparison between $\langle x_g \rangle$ and $\langle T_c - T_g \rangle$ for different angles indicates that the variations in the time averaged concentration next to the center of the wire were responsible for the variation of the time averaged temperature rise. If mixing within the channel were such that no gradients in the concentration existed, the value of $\langle T_c - T_g \rangle$ would have been about 475°C for these experiments.

E. Probability Density Functions

The probability density function (pdf) of the concentration fluctuations were measured at various angles using the aspirating probe. Figure 5.6 shows that the pdf's are slightly skewed, with the position of the mode relative to the average depending on the angular position of the distributor.

Measurements of the temperature fluctuations' pdf during the oxidation of hydrogen in excess air are shown in Figure 5.7. A 0.075 mm diameter wire was used and x_g was 0.025.

The pdf's are skewed and the relative position of the mode with respect to the average resulted to be as that found for the concentration fluctuations' pdf.

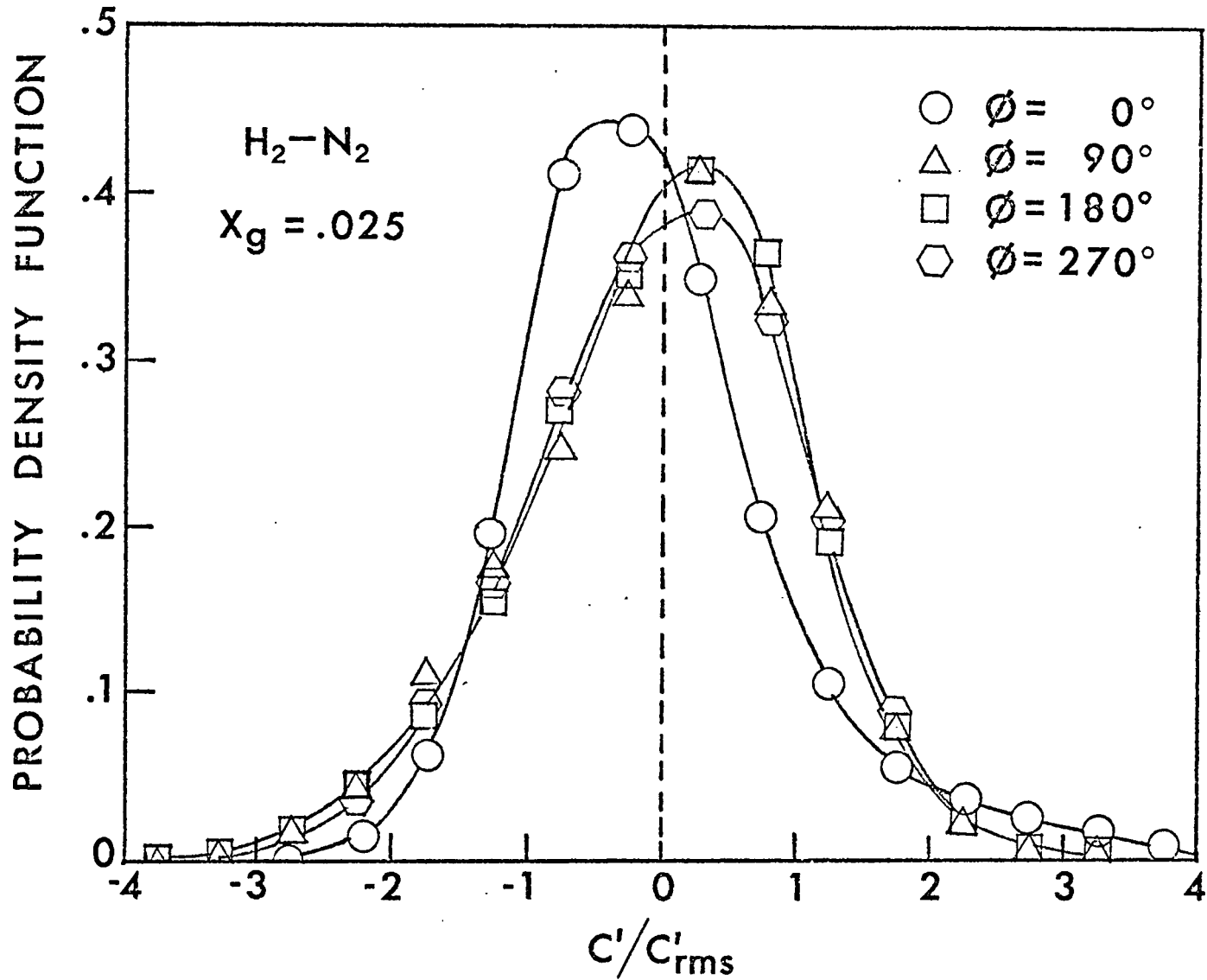


Figure 5.6 - Probability density function of hydrogen concentration fluctuations ($N_{Re} = 4000$, $T_g = 24^\circ C$)

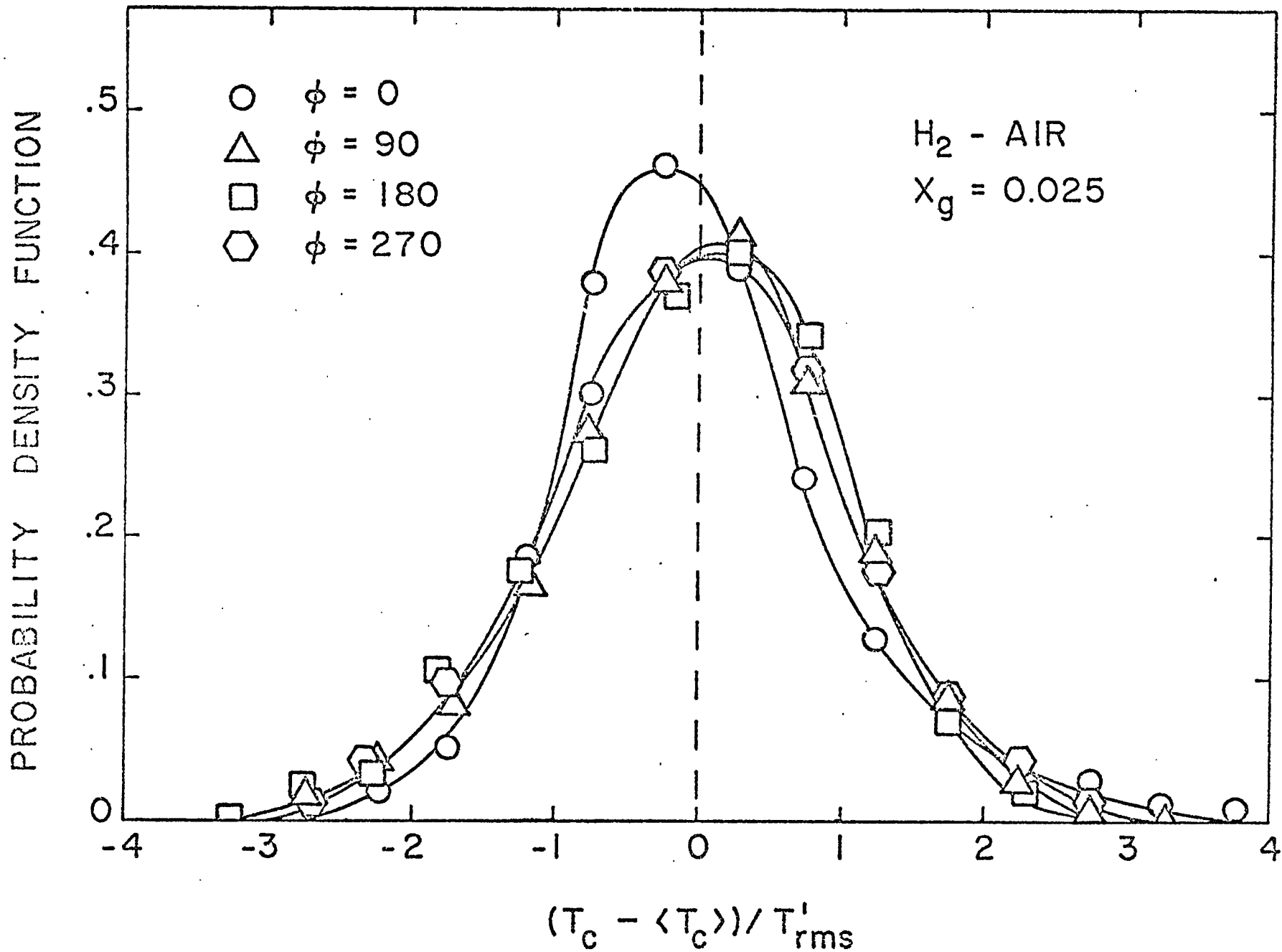


Figure 5.7 - Probability density function of temperature fluctuations.
 ($N_{Re} = 4000, T_g = 24^\circ C, d_w = 0.075mm$)

The strong similarity between the two probability density functions over a wide range of fluctuations intensity supports the argument that the temperature oscillations are induced by the concentration fluctuations.

Figure 5.8 shows the pdf of the turbulent velocity fluctuations for a channel Reynolds number of 4000. It is skewed to the left so that the most probable value occurs at velocities lower than the average.

Comparison with the pdf's shown in Figure 5-6 indicates that for hydrogen oxidation, the sign of of the velocity-concentration cross correlation, R_{uc} , depends on the angle of injection. It will be shown later in this Chapter that not only the sign of R_{uc} , but also its magnitude depend on the angle ϕ .

F. Effect of Wire Diameter

Experiments were carried out with wires of different diameters while feeding hydrogen at point A for two different angles of injection. The rms of the temperature fluctuations in each case was used to check the validity of Eq. (5-1).

The results are reported in Tables 5.2 and 5.3. The values of τ were determined from independent heat transfer experiments.

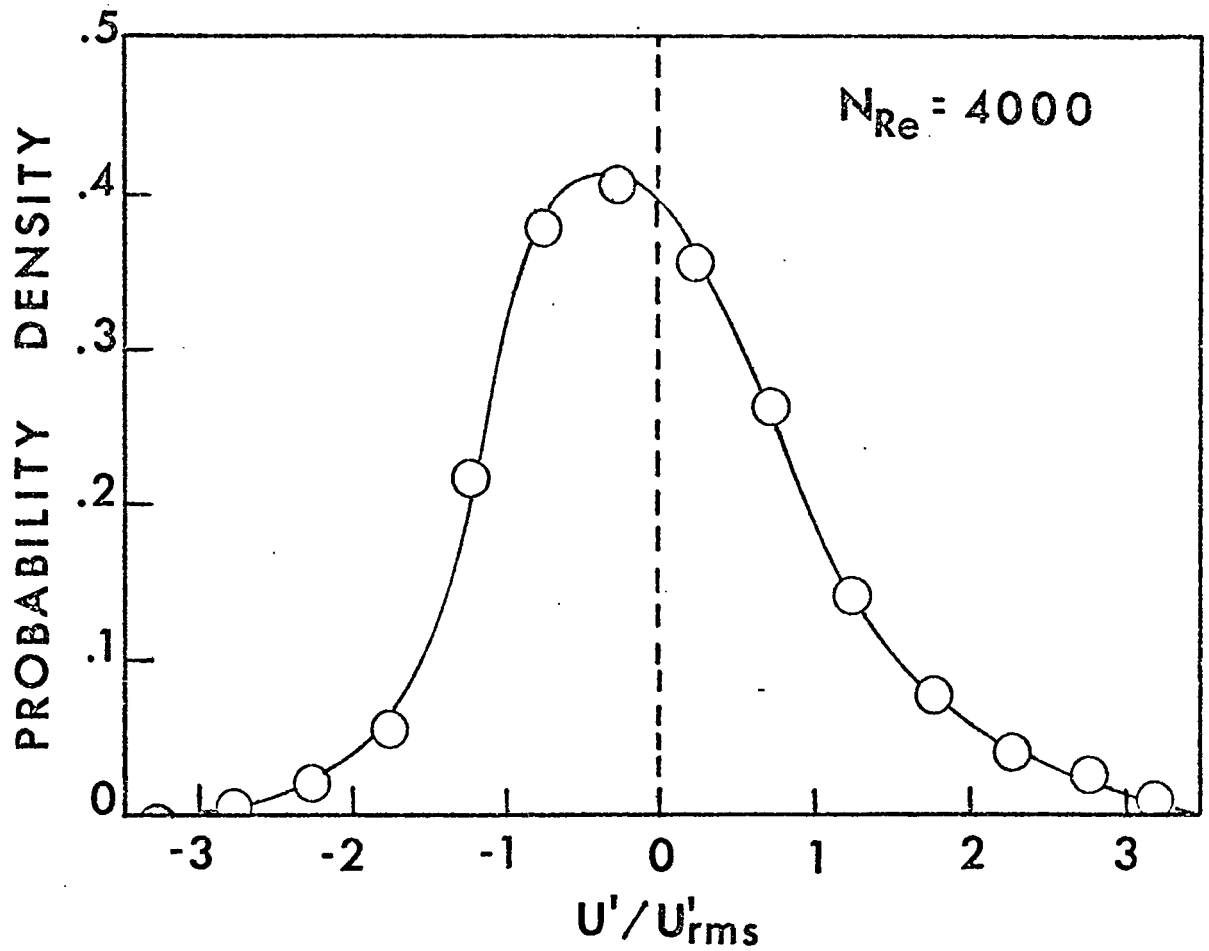


Figure 5.8 - Probability density function of air turbulence ($T_g = 24^\circ\text{C}$)

TABLE 5.2

Calculated hydrogen fluctuations for

$$\phi = 180^\circ (\tau_c = 0.039 \text{ sec})$$

wire diameter [mm]	τ [sec]	$T'_{rms}/\langle T_c - T_g \rangle$	$\frac{c'_{rms}}{\langle c \rangle}$ (Eq. 5.1)
0.125	0.141	.015	.033
0.075	0.070	.017	.028
0.025	0.011	.025	.029

TABLE 5.3

Calculated hydrogen fluctuations for

$$\phi = 270^\circ (\tau_c = 0.030 \text{ sec})$$

wire diameter [mm]	τ [sec]	$T'_{rms}/\langle T_c - T_g \rangle$	$\frac{c'_{rms}}{\langle c \rangle}$ (Eq. 5.1)
0.125	0.141	.025	.058
0.075	0.070	.034	.061
0.025	0.011	.046	.053

For a given injection angle, the value of $T'_{rms}/\langle T_c - T_g \rangle$ almost doubled when the wire diameter was decreased from 0.125 mm to 0.025 mm. However, the computed magnitude of the concentration fluctuations remained nearly constant for a given angle ϕ .

Figure 5.9b shows that for a given angle of injection, $c'_{rms}/\langle c \rangle$ is independent of the wire diameter used to measure $T'_{rms}/\langle T \rangle$. The data presented in Figure 5.9-b, yields values of $c'_{rms}/\langle c \rangle$ which deviate no more than 4% from the measurements of the concentration fluctuations obtained with the aspirating probe.

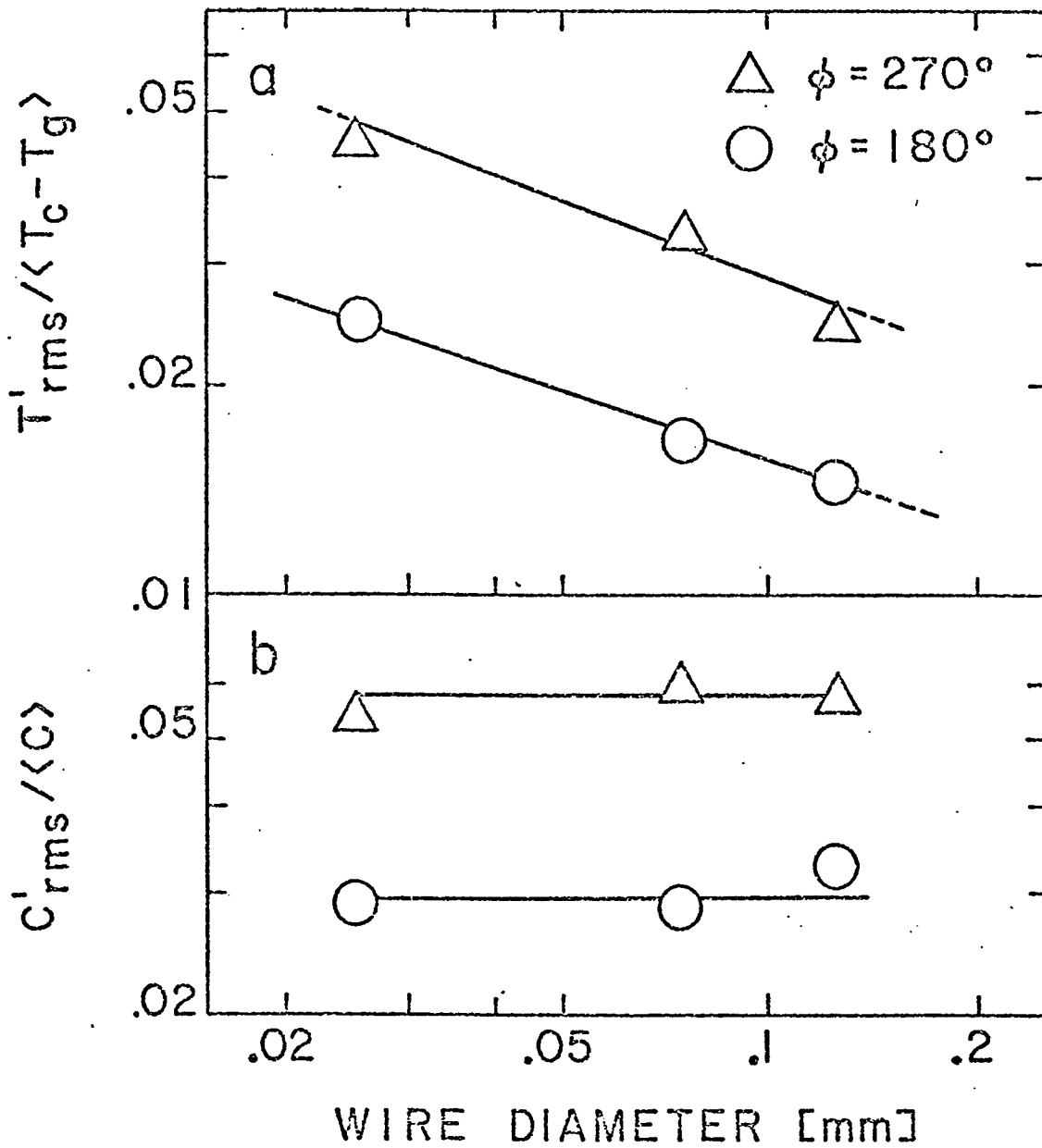


Figure 5.9

- a) Effect of wire diameter and position of distributor on the temperature fluctuations for a mixture of 2.5%v H_2 in air
- b) Computed values of $c'_{rms}/\langle c \rangle$ from $T'_{rms}/\langle T_c - T_g \rangle$ using equation (5-1)

These results strongly support the validity of equation 5-1 and the model which predicts that, when the capacity term is large, temperature fluctuations are induced mainly by concentration fluctuations in the reacting gas mixture.

G. Power Spectral Density Functions

To check the validity of the pseudo-steady state model, the spectral density function (sdf) of the temperature fluctuations at the center of a .025 mm diameter wire was determined as shown in Figure 5.10. Hydrogen oxidation was the reaction taking place and the angle of injection corresponds to $\phi = 180^\circ$.

The predicted behavior (solid line) can be obtained from the pseudo-steady state model by substituting Eqs. (2-81) and (2-82) into (2-80). This yields

$$\frac{G_{T'}(f)}{G_{T'}(0)} = \frac{1}{[1 + (2\pi f\tau)^2][1 + (2\pi f\tau_c)^2]} \quad (5-2)$$

where

$$G_{T'}(0) = 4(\tau_c + \tau)\langle T'^2 \rangle \quad (5-3)$$

Figure 5-10 shows that the experimental sdf does not follow the prediction of Eq. (5-2) very well. The peak that appears between 3 and 4 Hz originally was believed to be due to an inherent vibration of the channel assembly. In order to test this assumption, hydrogen was fed at point C (Figure 3.1) and the sdf was determined for a 0.025 mm diameter wire.

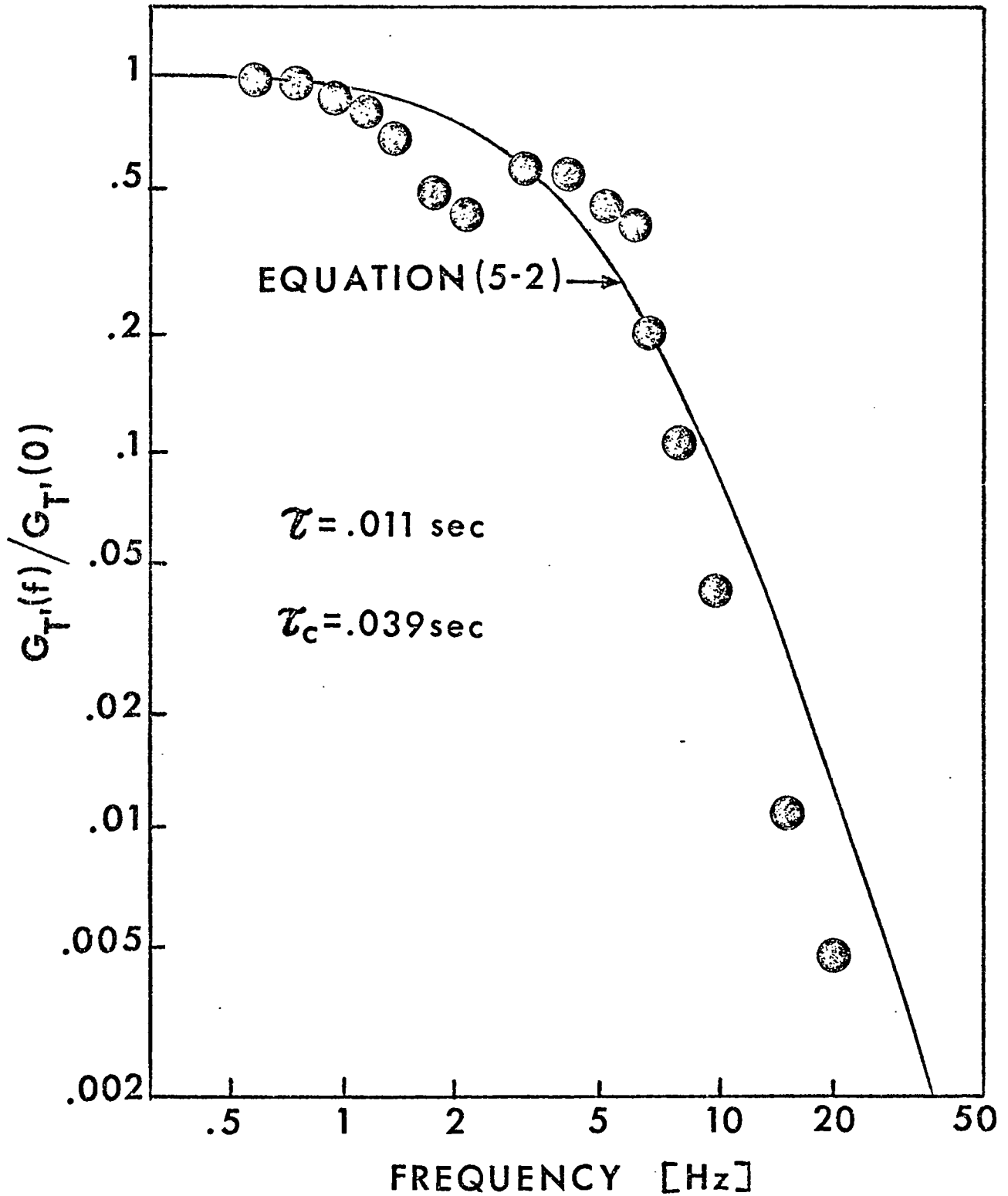


Figure 5.10

Normalized spectral density function of temperature fluctuations during hydrogen oxidation ($d_w = 0.025 \text{ mm}$, $\phi = 180^\circ$, $x_g = .025$, $T_g = 24^\circ\text{C}$)

The results are shown in Figure 5.11 (upper curve). For this experiment, the T'_{rms} was close to 1.7°C or about eight times smaller than T'_{rms} observed during the experiments that led to Figure 5.10. If periodic vibrations of significant magnitude were actually inherent to the system, the peak that appeared in Figure 5.10 should have been present in the latter spectrum. However, the data show that this was not the case.

The other sdf shown in Figure 5.11 (lower curve) corresponds to experiments reported by Edwards [4] using a 0.075 mm diameter wire and feeding hydrogen ($x_g = 0.030$) at point C. The measured T'_{rms} was 1.1°C and the data do not show any significant peaks over the range of frequencies of interest.

These observations lead to the conclusion that in the presence of concentration gradients at the wire station, the normalized spectrum of the temperature fluctuations does not follow the prediction of Eq. 5-2.

Figure (5-12) shows the normalized power spectrum for a 0.075 mm diameter wire with $x_g = 0.075$ hydrogen in air and $\phi = 270^{\circ}$. An unexpected trend of the data (between $f \approx 0.6$ Hz and $f \approx 4$ Hz) was observed. For higher frequencies the data agree very well with the theoretical prediction of Eq. (5-2).

The above discussion indicates that the influence of concentration gradients on the sdf depends not only on the injection angle ϕ , but also on the wire diameter. Unfortunately, an exact

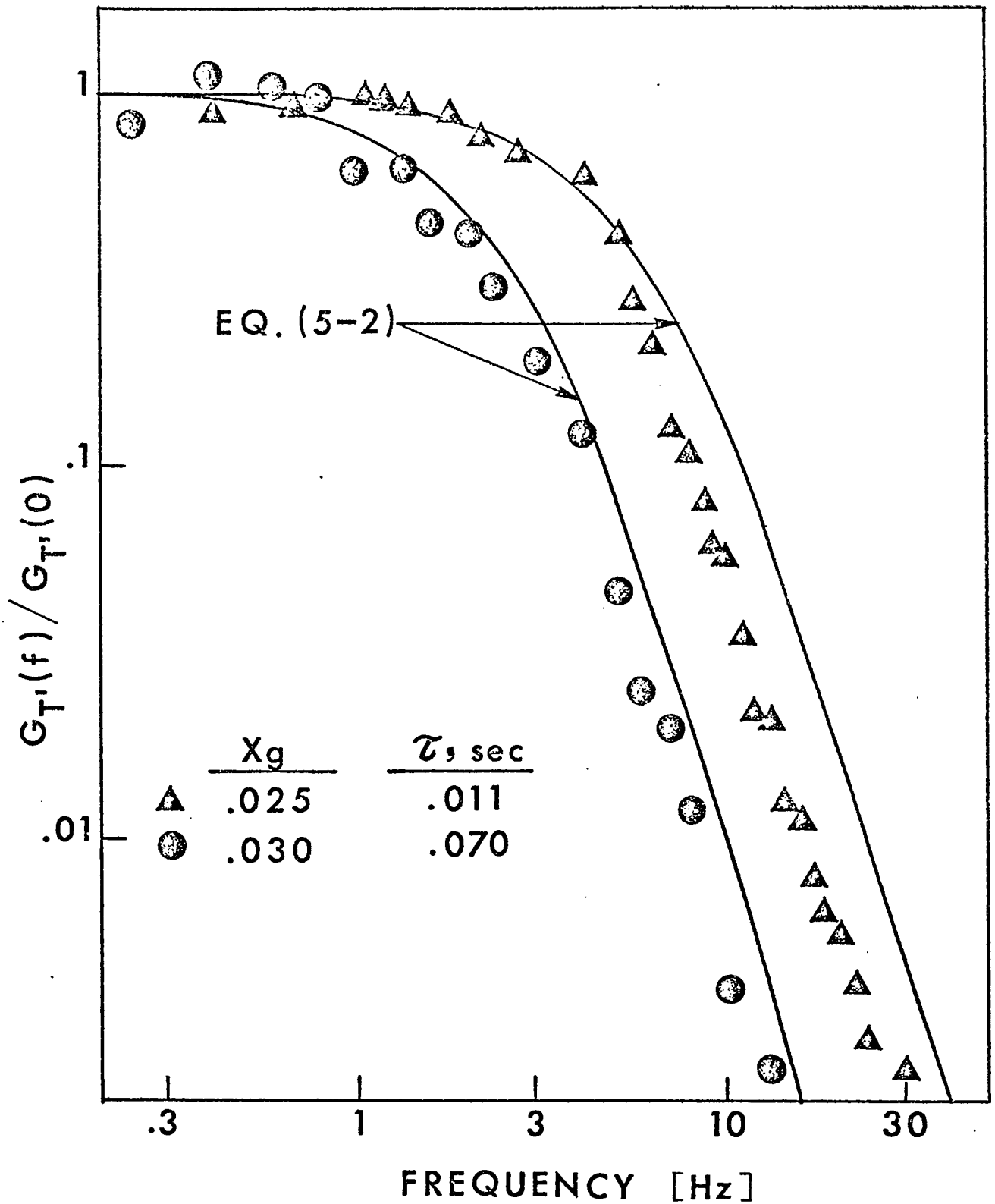


Figure 5.11

Normalized spectral density function of temperature fluctuations during the oxidation of either hydrogen or ammonia in air ($\tau_c = 0.030$ sec, $N_{Re} = 4000$, $T_g = 24^\circ\text{C}$)

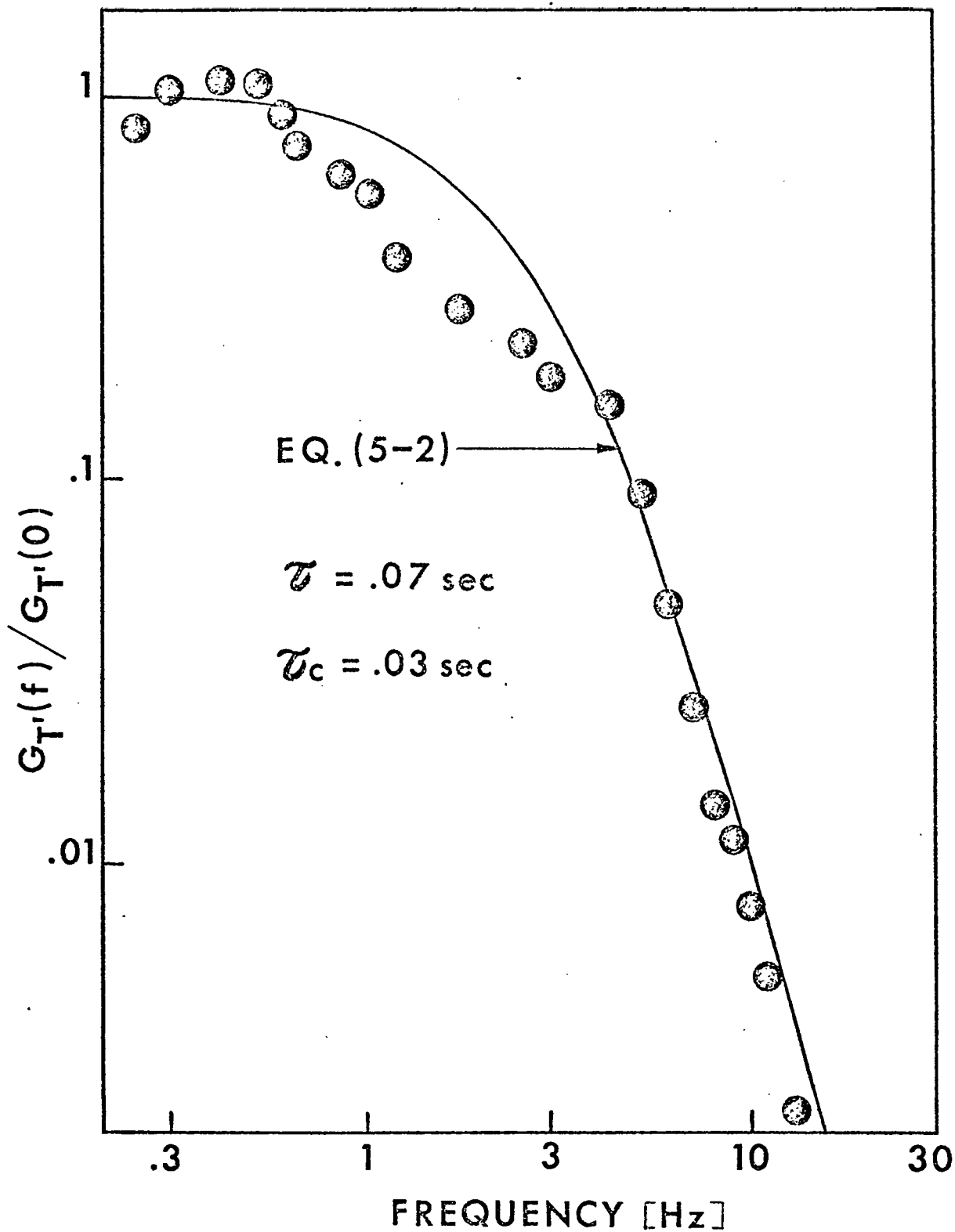


Figure 5.12

Normalized spectral density function of temperature fluctuations during hydrogen oxidation ($d_w = .075 \text{ mm}$, $\phi = 180$, $x_g = .025$, $T_g = 24^\circ\text{C}$)

explanation which will predict the observed irregularities is not available at present.

When hydrogen was fed at point C the flickering was reduced about eight times due to better mixing of the reactants. Figure 5-11 shows that when concentration gradients are absent, the spectral density functions agree well with the theoretical curves (especially for $d_w = 0.075$ mm). The upper curve, corresponding to a smaller wire diameter (0.025 mm), shows a rather marked difference between the experimental points and the prediction of Eq. (5-2). Experiments were carried out using a smaller probe ($l_w \approx 7$ mm) to hold the 0.025 mm diameter wire. For this case, the wire time constant, τ , was calculated to be 0.0095 sec. The power spectrum is shown in Figure 5-13.

The agreement is a little better but still not satisfactory. The agreement between the experimental data and the theoretical prediction for this latter spectrum, is about equal to that for the case of the lower curve shown in Figure 5.11.

It is evident that the spectral density functions in contrast to rms and pdf measurements were not useful for determining the principal cause of flickering. Nevertheless, we must remember that the validity of the solid lines shown in Figures 10 through 13 depends upon the assumption that Eq. (2-81) is a good approximation for the spectrum of concentration fluctuations.

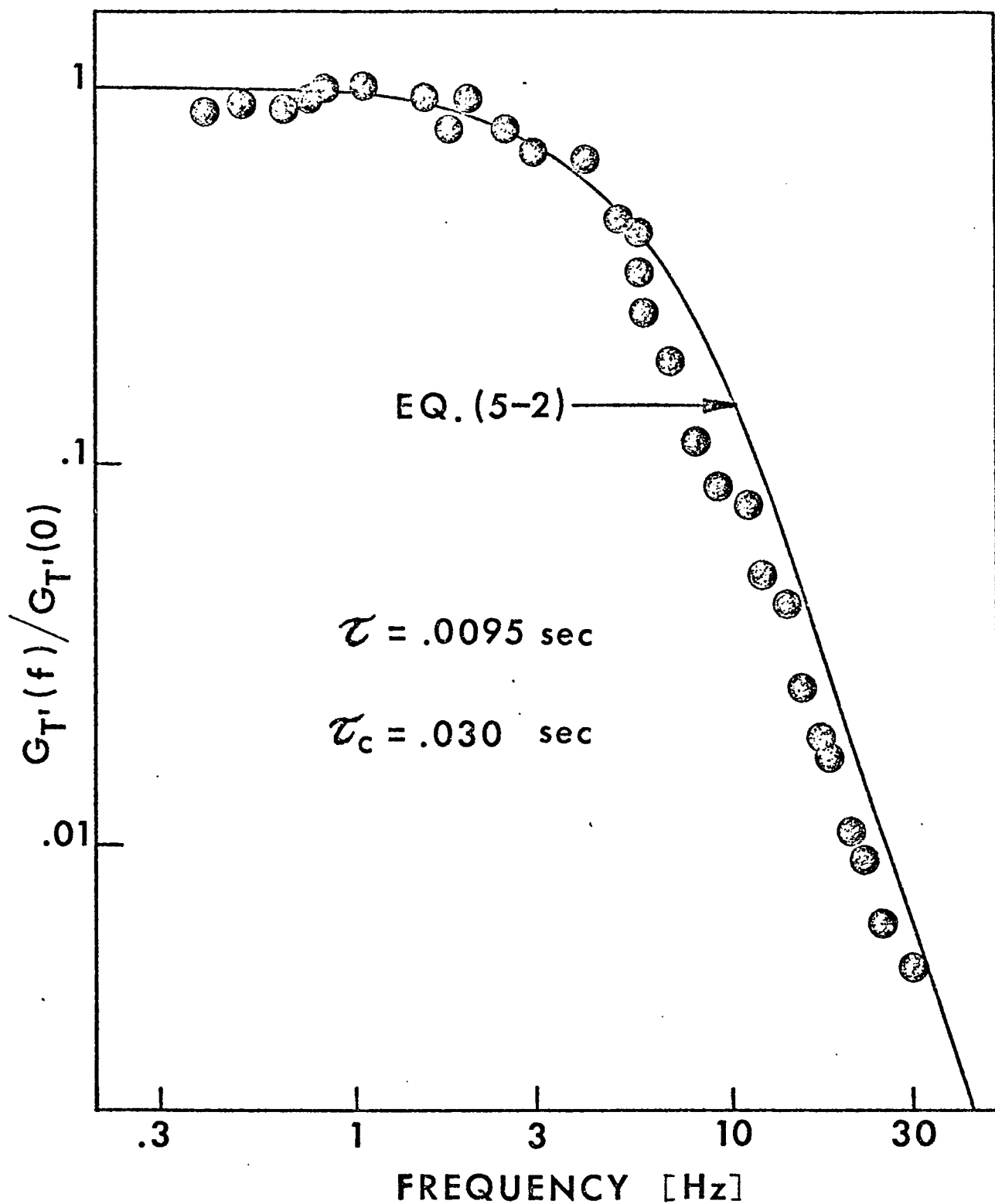


Figure 5.13

Normalized power spectrum of temperature fluctuations during hydrogen oxidation ($x_g = .025$, $d_w = .025 \text{ mm}$, $N_{Re} = 4000$, $T_g = 24^\circ\text{C}$)

Several experiments were made with the aspirating probe to check that assumption. Hydrogen (2.5%v) was mixed with a stream of nitrogen using different feed ports. The results are presented in Figure 5-14 and 5-15.

Equation (2-81) can be rewritten as

$$\frac{\pi f_{1/2} G_{c'}(f)}{2 \langle c'^2 \rangle} = \frac{1}{1 + \left(\frac{f}{f_{1/2}}\right)^2} \quad (5-4)$$

where the Eulerian concentration time scale, τ_c , has been taken as

$$\tau_c = 1/(2\pi f_{1/2}) \quad (5-5)$$

by analogy with equation (2-77).

The solid line in Figures 5-14 and 5-15 corresponds to the assumption of Equation (5-4). The agreement of the experimental data is good for high frequencies and $\phi = 90^\circ$ when feeding at point A.

In general, an unexpected behavior appears in the three spectra shown in Figure 5-14 for low frequencies. This must be due to the concentration gradients in the channel. The experimental data for $\phi = 180^\circ$ and $\phi = 0^\circ$ and high frequencies fell below the theoretical curve.

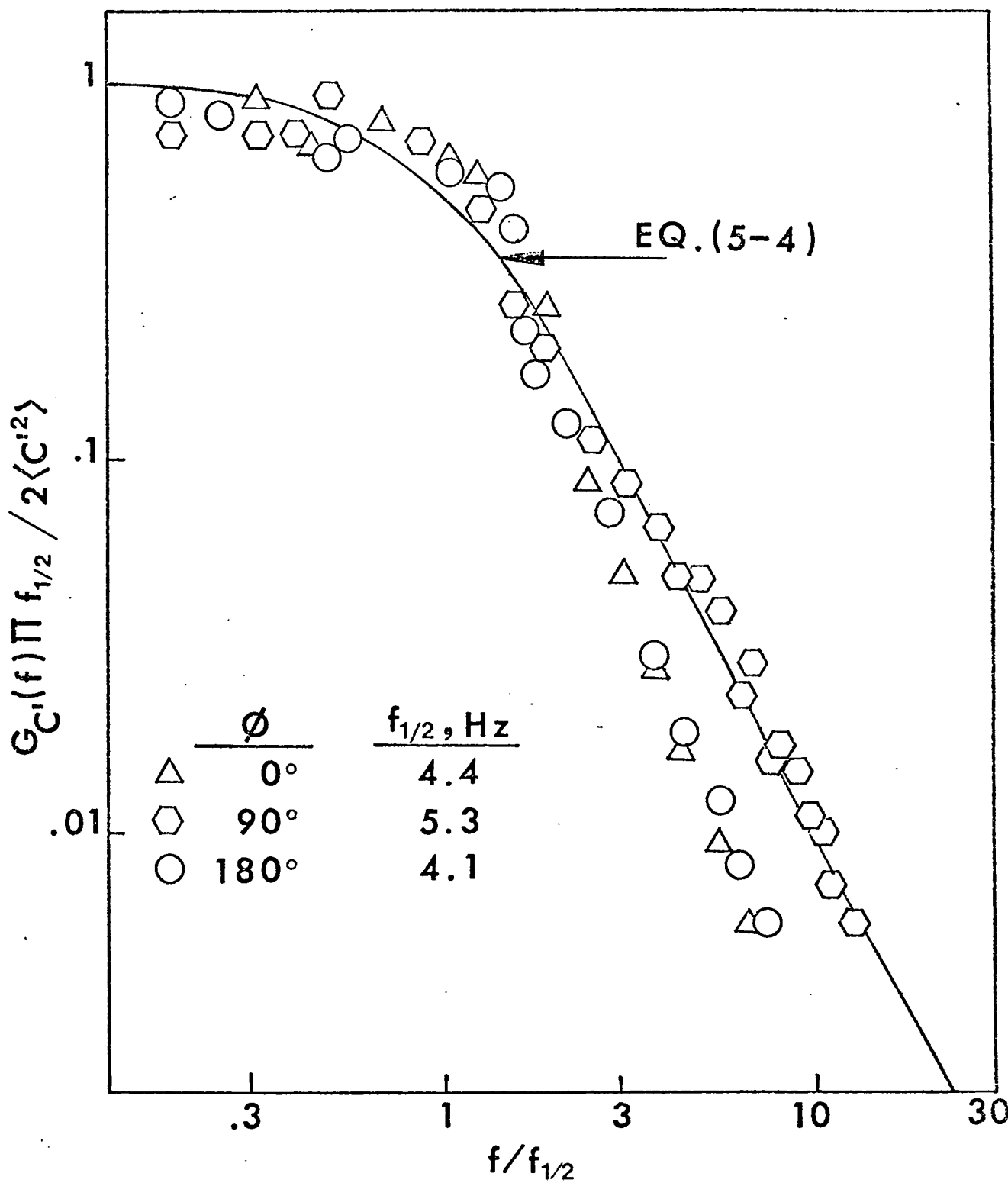


Figure 5.14

Power spectral density of hydrogen concentration fluctuations
 ($N_{\text{Re}} = 4000, x_g = .025, T_g = 24^\circ\text{C}$)

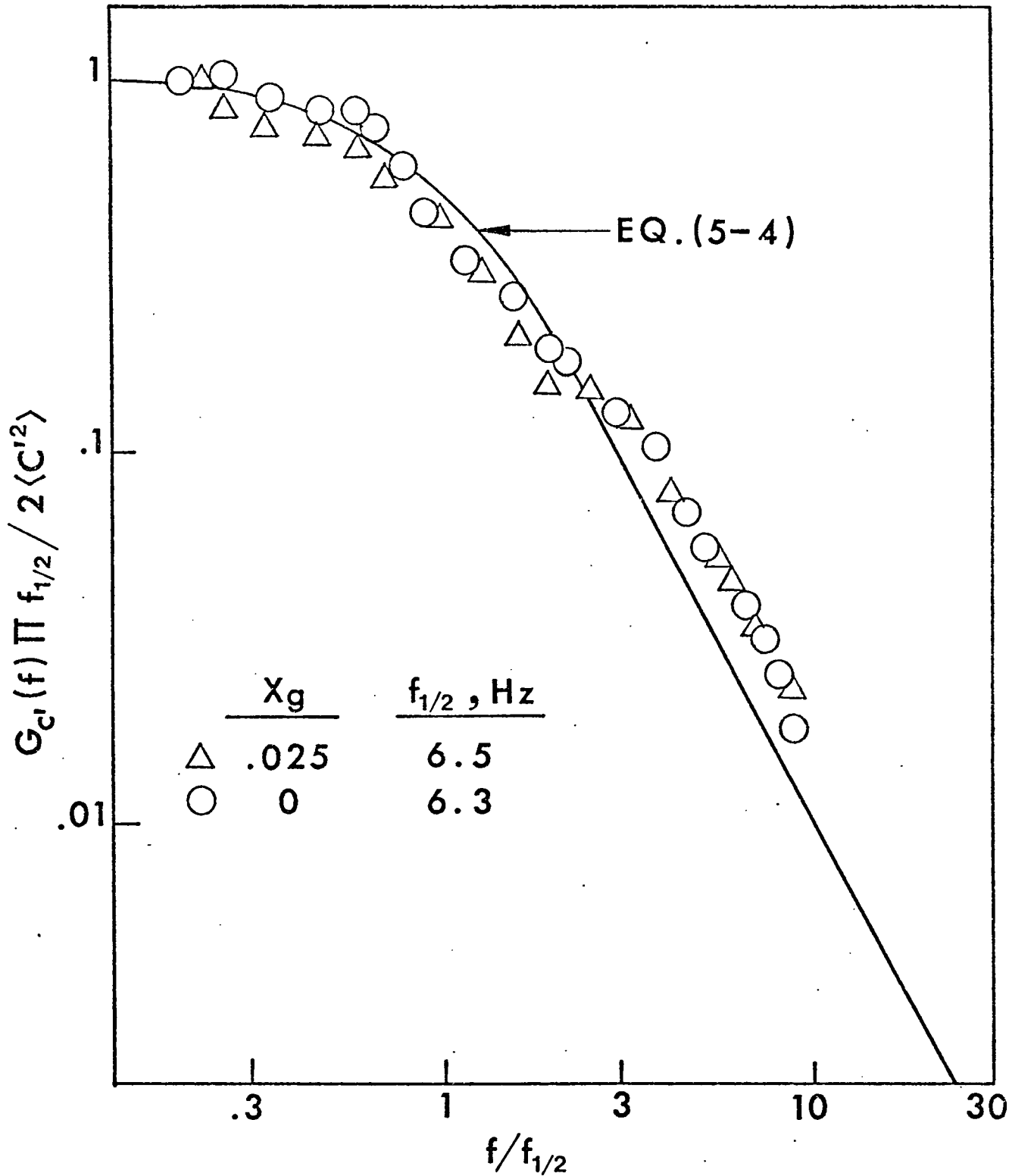


Figure 5.15

Power spectral density of hydrogen concentration and pressure fluctuations ($N_{Re} = 4000$, $T_g = 24^\circ\text{C}$)

For low intensity of concentration fluctuations (point C) the measured spectrum resulted as shown in Figure 5.15. At $(f/f_{1/2})$ of about 2, a sudden change from below to above the theoretical curve was observed. This profile is very similar to that predicted but the agreement is not satisfactory.

It is important to point out that when hydrogen was not injected at all ($x_g = 0$), a power spectrum almost identical to the first one was obtained. This means that for small concentration fluctuations (point C), the aspirating probe measurements may be affected by pressure fluctuations of the nitrogen stream.

Fortunately, the constants that appear in Eq. 2-82 are rather insensitive to the exact form of the concentration sdf. This is often the case when dealing with results based on integrals of assumed profiles. Therefore, Eq. 5-1 is still a valid expression for checking the cause of flickering even when Eq. (5-4) is not a good representation of the concentration sdf.

H. Ammonia-Air Experiments

A mixture of 5% v ammonia in air was used to study ammonia oxidation on the surface of a 0.075 mm diameter wire. Temperature fluctuations were measured with the infrared detector while feeding ammonia through point A.

Two geometrically similar distributors with different feed injection holes were used. The distributor used for the H_2 -air experiments (.34 mm diameter holes) was denoted as #1 and distributor #2 had identical outside diameter and length but larger injection holes (.51 mm diameter).

Figure 5-16 describes the effect of the injection angle and the size of the holes on both T'_{rms} and $\langle T_c - T_g \rangle$ for a channel Reynolds number of 4000. The minimum fluctuation intensity corresponds to $\phi = 180^\circ$ for both distributors in accordance with the results obtained for the hydrogen oxidation.

The location of the maxima for these curves, however, appears at different angular positions as compared with the results of the hydrogen-air reaction. This must be due to a different effect of ϕ and hole diameter on the ammonia concentration fluctuations.

Unfortunately $c'_{rms}/\langle c \rangle$ for ammonia can not be measured by the aspirating probe due to the small difference in thermal conductivities of air and ammonia.

During these ammonia oxidation experiments the rms of the fluctuations ranged from 12.2°C to 26°C for distributor #1 and from 8.9°C to 25.6°C for distributor #2, both ranges being a little smaller than for the case of the hydrogen air experiments.

It is important to mention that when the distributor at point A was used to obtain the 2.5% v mixture of hydrogen in air, the injection momentum of the jets was $1.14 \text{ gr/cm}^2\text{-sec}$. However, when the NH_3 (5.0% v) was fed at the same point the injection momenta were 19.8 and $8.9 \text{ gr/cm}^2\text{-sec}$ for the jets from distributions #1 and #2 respectively.

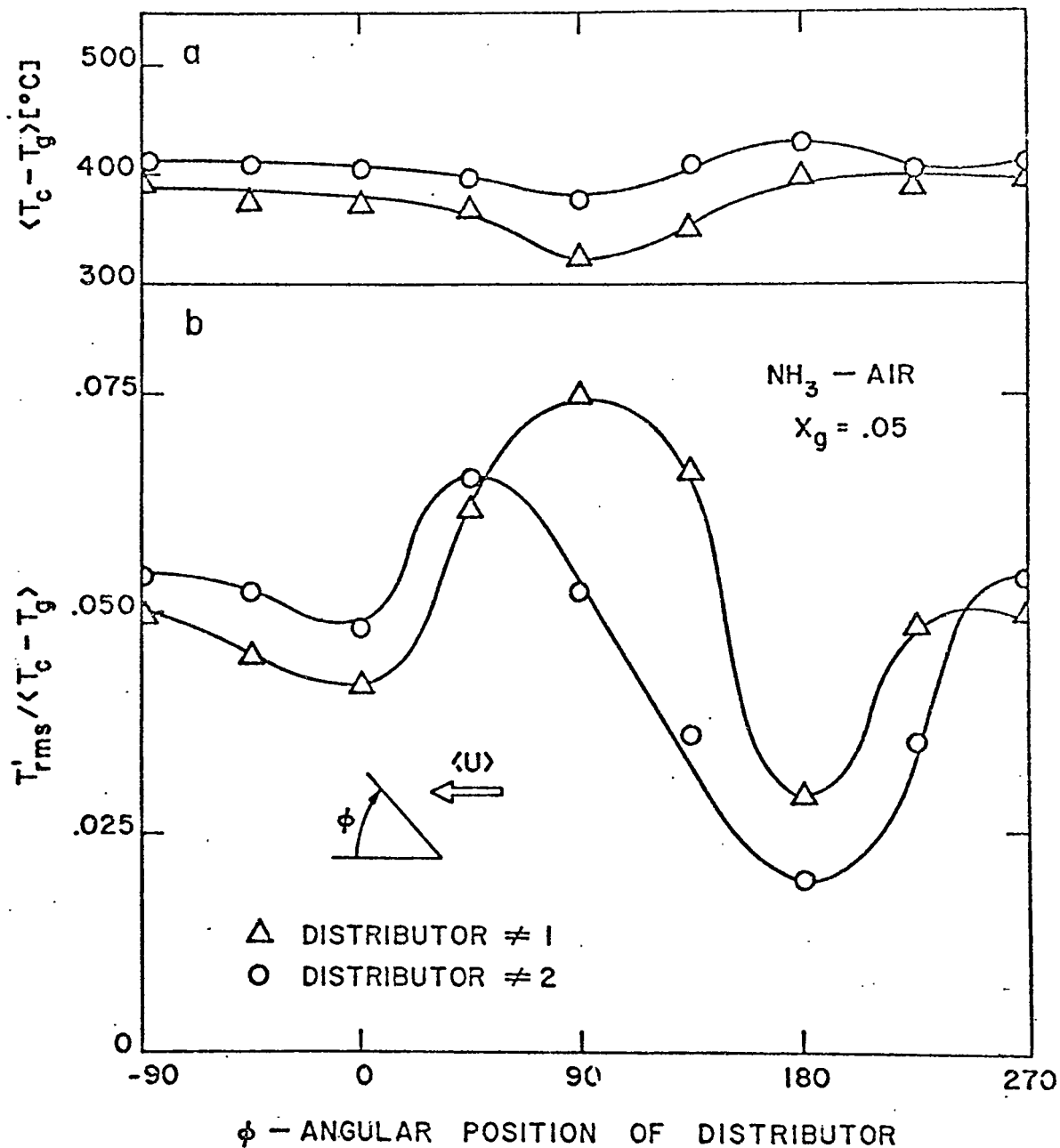


Figure 5.16

Effect of the angular position and size of the holes of the distributor on the magnitude of $T'_{rms} / \langle T_c - T_g \rangle$ and $\langle \Delta T_{ad}^* \rangle$ for ammonia oxidation ($d_w = 0.075$ mm, $T_g = 24^\circ C$)

These differences in the injection momenta of the jets were responsible for the variation in the effect of the angle ϕ on the concentration fluctuations of the mixtures.

I. Constant Temperature Experiments

When temperature fluctuations arise due to incomplete mixing of the reactants, flickering can be used as a measure of concentration fluctuations by applying the pseudo steady-state model to a wire operating at constant temperature.

To test this hypothesis, hydrogen (2.5% v) was fed into the reactor at point A using the standard distributor. The reaction was sustained on a .005 mm diameter wire connected to a Thermo-Systems Inc. constant temperature anemometer.

Equation 2-56 was rewritten as

$$y = a + bx \quad (5-6)$$

where

$$y = \frac{100}{m} \left[\frac{\langle (20e)^2 \rangle}{\langle E \rangle^2} - \frac{\langle (5fu')^2 \rangle}{\langle u \rangle^2} \right] \quad (5-7)$$

$$x = m/10 \quad (5-8)$$

$$a = -10^4 \left\langle \frac{fu'}{\langle u \rangle} \frac{C'_g}{\langle C'_g \rangle} \right\rangle \quad (5-9)$$

$$b = 10^5 \frac{\langle C'_g{}^2 \rangle}{\langle C'_g \rangle^2} \quad (5-10)$$

In deriving Eq. (5-6), the value of the constant n in Eq. (2-56) was taken as 0.5 from the results of turbulence experiments made with a geometrically similar hot sensor (see Appendix II).

The angle of injection was varied and for each ϕ the system was operated at three different values of m . A graph of y (Eq. 5-7) vs. x (Eq. 5-8) was drawn and from the slope and intercept of the "best fit" straight line $c'_{rms}/\langle C_g \rangle$ and R_{uc} were calculated.

The experimental data for different angles are shown in Figure 5-17. The final results are compared with Table 5-4 with the measured values of $c'_{rms}/\langle C_g \rangle$ using the aspirating probe and the calculated values from Eq. 5-1.

TABLE 5.4

Hydrogen fluctuations $c'_{rms}/\langle c \rangle$
evaluated by three different methods
($x_g = 0.025$)

Angle ϕ (Degrees)	Measured with asp. probe	Calculated by Eq. (5-1)	Measured at constant T
135	0.040	.051	0.053
180	0.029	.028	0.032
225	0.038	.034	0.039

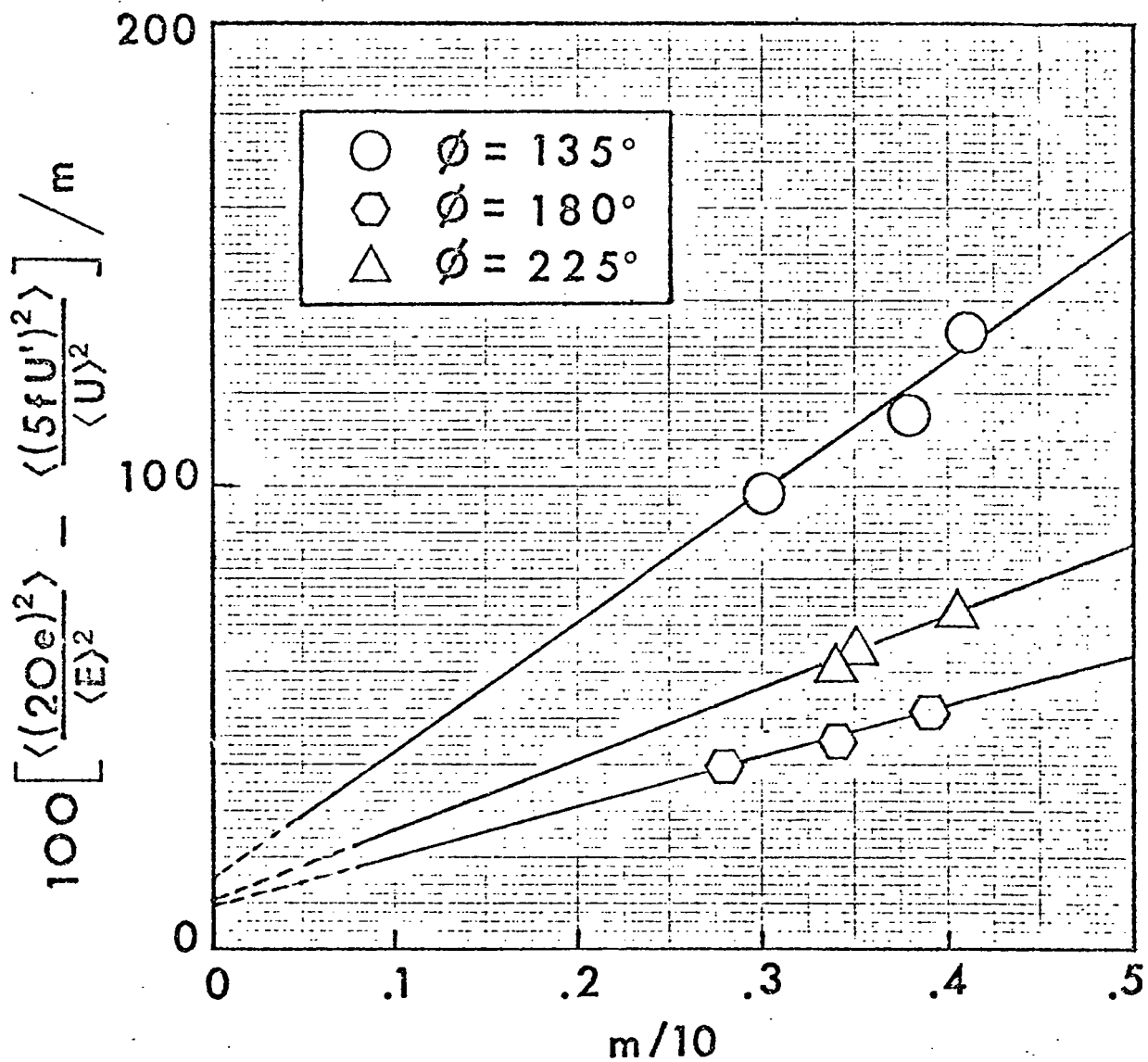


Figure 5.17

Correlation of electrical overheat results for constant temperature operation according to the pseudo-steady state model

In general, the results of the constant temperature technique yielded values higher than those obtained by the other two methods. The agreement with either the aspirating probe measurements or the values from Eq. (5-1) depends on the angle ϕ .

However, the order of magnitude of $c'_{rms}/\langle c \rangle$ for a given angle ϕ remains the same regardless of the method used. Furthermore, the relative change in the intensity of $c'_{rms}/\langle c \rangle$ as ϕ is varied follows the same trend for the three cases.

Values of $c'_{rms}/\langle c \rangle$ using the constant temperature method are not reported for $225^\circ < \phi < 135^\circ$ due to the difficulty in obtaining consistent data in that range. As $c'_{rms}/\langle c \rangle$ increases the determination of m (Eq. 2-54) becomes very inaccurate and the results obtained were not at all reliable.

The velocity concentration cross correlation, R_{uc} , was experimentally determined for the hydrogen oxidation at different angles of injection. This correlation is defined as

$$R_{uc} = \langle u'c' \rangle / u'_{rms} c'_{rms} \quad (5-11)$$

and it is bounded by

$$-1 \leq R_{uc} \leq +1 \quad (5-12)$$

The results are reported in Table 5-5.

TABLE 5.5

Experimental values of R_{uc}
for hydrogen oxidation

Angle ϕ (Degrees)	R_{uc}
135	-0.96
180	-0.86
225	-0.77

The negative sign for R_{uc} in this range of angles of injection agrees with the prediction made in Section E when the probability density functions shown in Figure 5-6 and 5-8 were compared.

These experiments indicate that a constant temperature hot wire can be used for measuring concentration fluctuations and R_{uc} in the presence of a mass-transfer limited reaction.

CHAPTER VI

CONCLUSIONS AND RECOMMENDATIONS

When a mass transfer limited chemical reaction occurs on the surface of a single catalytic wire, the results of this work indicate that:

- 1) The observable temperature fluctuations are induced mainly by concentration fluctuations in the reacting mixture. Thus, it is important to improve the gas mixing in commercial operations in order to reduce the rate of precious metal loss.
- 2) Flickering can be used as a means of measuring concentration fluctuations. At the present time, measurements of this type are limited to a very few substances for which the existing probes can give an accurate response. Hence, the development of a "reacting probe" would extend the number of mixtures that can be used in studies of concentration fluctuations.

Recommendations for future work

Further studies should be undertaken to check the validity of Eq. (5-2) as the appropriate spectral representation for the phenomenon taking place on the catalytic wires.

To this end, it would be desirable to install a converging section at the entrance of the reactor in order to obtain a more homogeneous composition profile, yet allowing injection close to the wire station.

These tests should be carried out with wires of very small diameter (.025 mm or less) for which $\tau < \tau_c$, thus increasing the sensitivity of the theoretical curve to the behavior of the concentration fluctuations.

The application of the constant temperature hot wire with reaction must be extended to higher intensities of $c'_{rms}/\langle c \rangle$. New methods for determining the parameter \underline{m} under those conditions will have to be examined.

Another area where further work may be directed refers to studies of flickering on laboratory scale gauzes. The pertinent theoretical model has already been developed to this effect.

NOMENCLATURE

a	capacity term defined by Eq. (2-10)
A	wire cross section, cm^2
A(g)	reactant A concentration in fluid, g mole cm^{-3}
AS	occupied catalytic sites, g mole cm^{-2}
B(g)	product B concentration in fluid, g mole cm^{-3}
$C_{g,c}$	reactant concentration in fluid, g mole cm^{-3}
C_p	wire heat capacity, $\text{cal g}^{-1} \text{ }^\circ\text{K}^{-1}$
C_{pf}	fluid heat capacity, $\text{cal g}^{-1} \text{ }^\circ\text{K}^{-1}$
d	wire diameter, cm
D	diameter, cm
D_{AB}	binary diffusion coefficient, $\text{cm}^2 \text{ sec}^{-1}$
e	fluctuating component of voltage, volts
E	voltage, volts
E_1	one dimensional spectral density of turbulence, $\text{cm}^2 \text{ sec}^{-1}$
E_m	metal loss activation energy, cal g mol^{-1}
f	frequency, Hz
	dimensionless factor, defined by Eq. (2-42)
$f_{1/2}$	half power frequency, Hz (Eq. 2-64)
f(r)	longitudinal correlation coefficient, (Eq. 2-68)
G_y	one-sided spectral density of random process y
h	heat transfer coefficient, $\text{cal sec}^{-1} \text{ cm}^{-2} \text{ }^\circ\text{K}^{-1}$
H	system transfer function
ΔH	heat of reaction, cal g mole^{-1}

i	fluctuating component of current, amperes
I	current, amperes
J	conversion constant, $\text{cal sec}^{-1} \text{ watt}^{-1}$
k_1	mass transfer and adsorption rate constant, $\text{cm}^3 \text{ g mole}^{-1} \text{ sec}^{-1}$
k_2	reaction and desorption rate constant, sec^{-1}
k_c	mass transfer coefficient, cm sec^{-1}
k	thermal conductivity, $\text{cal sec}^{-1} \text{ cm}^{-1} \text{ }^\circ\text{K}^{-1}$
K	constant defined in Eq. (2-9)
K_1, K_2	constants defined in Eq. (4-3)
ℓ	wire length, cm
L	total catalytic sites, g mole cm^{-2}
m	defined by Eq. (2-54)
M	weight of precious metal gauze, g
M_f	molecular weight of fluid, g g mole^{-1}
n	empirical velocity exponent in Eq. (2-34)
N_1	constant defined by Eq. (III-9)
N_2	constant defined by Eq. (III-10)
N_{Le}	Lewis number, $k_f/\rho_f D_{AB} C_{pf}$
N_{Nu}	Nusselt number, hD/k_f
N_{Pr}	Prandtl number, $C_{pf}\mu_f/k_f$
N_{Re}	Reynolds number, Du/v_f
N_{Sc}	Schmidt number, v_f/D_{AB}
N_{Sh}	Sherwood number, $k_c D/D_{AB}$
P	wire perimeter, cm

q	heat transfer rate, cal sec^{-1}
Q	volumetric flow rate, $\text{cm}^3 \text{sec}^{-1}$
r	surface reaction rate, $\text{g mole cm}^{-2} \text{sec}^{-1}$
$r(T)$	relative metal loss, Eq. (1-2)
R	gas constant, $\text{cal g mole}^{-1} \text{ } ^\circ\text{K}^{-1}$
R_w	wire resistance per unit length, ohm cm^{-1}
R_o	resistance per unit length at 0°C , ohm cm^{-1}
$R_E(\tau)$	Eulerian time velocity correlation
$R_T(\tau)$	Eulerian time temperature correlation
R_{uc}	velocity-concentration cross correlation
s	dimensionless position along wire axis
S	unoccupied catalytic sites, g mole cm^{-2}
t	time, sec
T	temperature, $^\circ\text{K}$
u	fluid velocity, cm sec^{-1}
x	position along wire axis, cm
x_c	position of wire center, cm
x_g	mole fraction of limiting reactant in fluid
y	random variable

Greek Symbols

α	constant defined by Eq. (III-24)
β	temperature coefficient of resistance, $^\circ\text{K}^{-1}$
η	fractional heat loss

ϵ	emissivity
λ	dimensionless parameter defined by Eq. (2-21)
ϕ	constant defined by Eq. (2-22)
θ_g	dimensionless gas temperature
θ_w	dimensionless wire temperature
Λ_f	longitudinal macroscale of turbulence, cm
μ	viscosity, $\text{g cm}^{-1} \text{sec}^{-1}$
ν	kinematic viscosity, μ/ρ , $\text{cm}^2 \text{sec}^{-1}$
ρ	wire density, g cm^{-3}
ρ_f	fluid density, g cm^{-3}
σ	Boltzman constant
τ_c	Eulerian time scale of concentration fluctuations, sec
τ_E	Eulerian time scale of turbulence, sec
τ_w	wire time constant, sec
τ_o	wire time constant with reaction, sec
ω	frequency, sec^{-1}

Subscripts

ad	adiabatic
b	bridge
c	convection
f	fluid
g	gas
k	conduction
m	maximum
r	radiation
w	wire

Superscripts

- ' fluctuating component about the mean value
- * with reaction only

Special Symbols

- (overbar) length average
- <> time average

BIBLIOGRAPHY

1. Nowak, E. J., Chem. Eng. Sci., 24, 421 (1969).
2. Ervin, M. A. and Luss, D., Chem. Eng. Sci., 27, 339 (1972).
3. Edwards, W. M., Worley, F. L., Jr., and Luss, D., Chem. Eng. Sci., 28, 1479 (1973).
4. Edwards, W. M., Ph.D. Thesis, University of Houston (1973).
5. Luss, D. and Ervin, M. A., Chem. Eng. Sci., 27, 315 (1972).
6. Hinze, J. O., Turbulence, McGraw-Hill Book Co., New York (1959).
7. Edwards, W. M., M.Sc. Thesis, University of Houston (1971).
8. McAdams, W. H., Heat Transmission, McGraw-Hill Book Co., New York (1954).
9. Bendat, J. S. and Piersol, A. G., Random Data: Analysis and Measurement Procedures, Wiley-Interscience, New York (1971).
10. Chen, C. F. and Hass, I. J., Elements of Control System Analysis, Prentice-Hall, Inc., New Jersey (1968).
11. Shelton, O. A., M.Sc. Thesis, University of Houston (1970).
12. Benedict, R. P., Fundamentals of Temperature, Pressure and Flow Measurements, John Wiley and Sons, Inc. (1966).
13. Bird, R. B., Steward, W. E., and Lightfoot, E.N., Transport Phenomena, Wiley International, Tokyo (1960).
14. Flow Corporation, "Selected Topics in Hot Wire Anemometer Theory", F. C. Bulletin No. 25.
15. Treybal, R. E., Mass Transfer Operations, McGraw-Hill Book Co., New York (1968).
16. Welty, J. R., Wicks, C. E., and Wilson, R. E., Fundamentals of Momentum, Heat and Mass Transfer, John Wiley and Sons, Inc. (1969).
17. Satterfield, C. N., Mass Transfer in Heterogeneous Catalysis, M.I.T. Press (1970).

APPENDIX I

CALIBRATION OF EXPERIMENTAL EQUIPMENT

1. Air flowmeter

Fisher & Porter Model No. 10A3565A

Serial No: 7102E1159B1

Tube No: FP-1-27-G-10/83

Float code: 1-GNSVT-64 T60

Listed calibration: 23.2 scfm of air @ 14.7 psia and 70°F

Metered calibration (reference [4]): 24.8 scfm of air at 14.7
psia and 70°F

In these experiments the actual calibration for air then
becomes

$$(\text{SCFM})_{\text{air}} = 24.8 \left(\frac{P_{\text{op}}}{14.7} \times \frac{530}{T_{\text{op}}} \right)^{1/2}$$

where

P_{op} = absolute pressure at operating conditions

T_{op} = absolute temperature at operating conditions.

The calibration curve is shown in Figure I.1 for $T_{\text{op}} = 24^{\circ}\text{C}$.

2. Nitrogen flowmeter

Fisher & Porter Model No. 10A3565A

Serial No.: 6811E1176B

Tube No.: FP-1-27-G-10/83

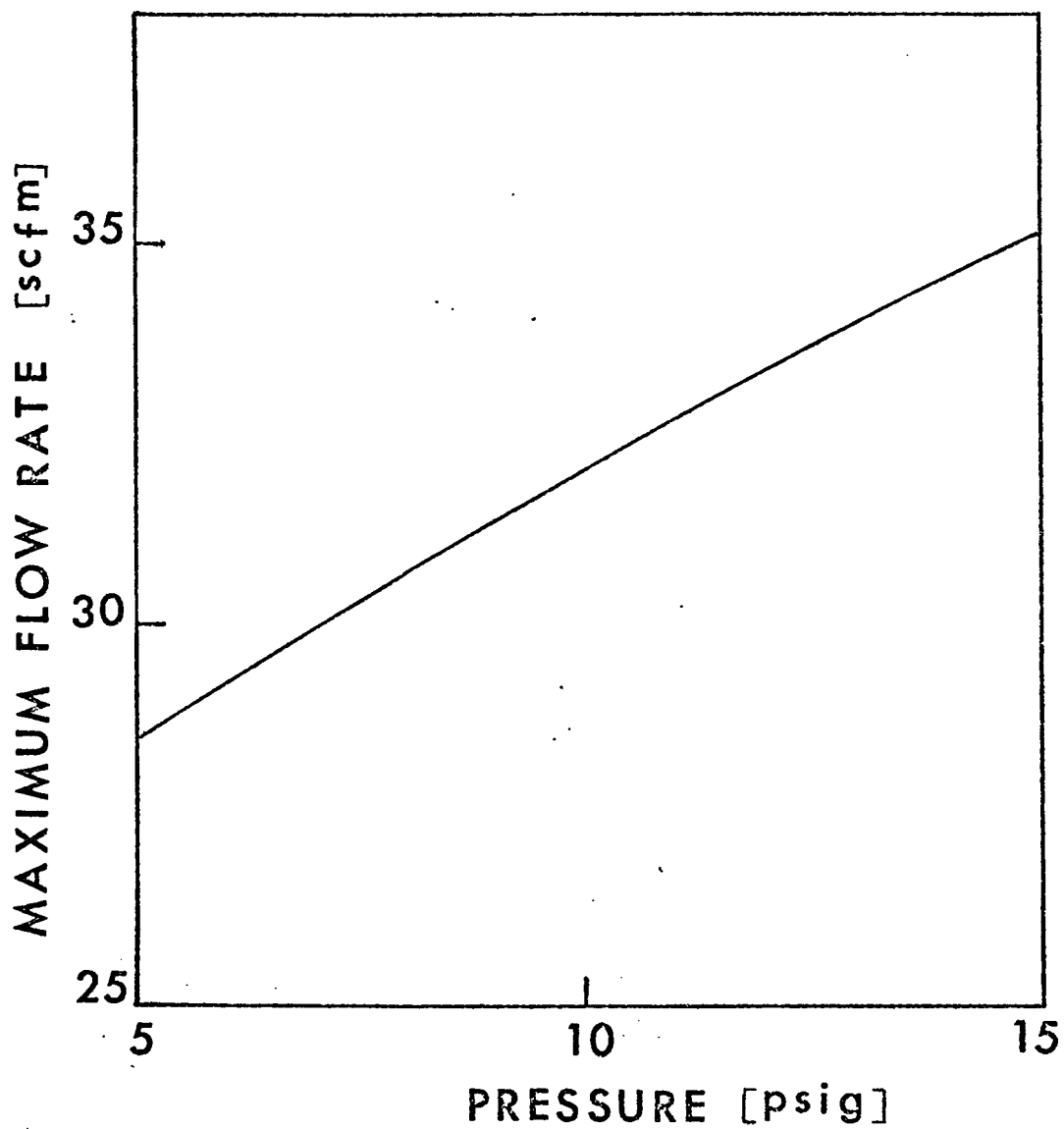


Figure I.1

Air flowmeter calibration ($T_g = 24\text{ C}$)

Float code: 1-GNSVT-64 (T60603D202)

Listed calibration: 23.2 scfm of air @ 14.7 psia and 70°F

Metered calibration: 24.8 scfm of air @ 14.7 psia and 70°F.

The actual calibration for nitrogen would be:

$$(\text{SCFM})_{\text{N}_2} = 25.2 \left(\frac{P_{\text{op}}}{14.7} \times \frac{630}{T_{\text{op}}} \right)^{1/2}$$

3. Ammonia flowmeter

Fisher & Porter Model No. 10A2735

Serial No.: 6804E1157B1

Tube No.: FP-1/2-27-G-10-10/83

Float code: 1/2 GUSVT-40 (603B204)

Listed calibration: 1.82 SCFM of air @ 14.7 psia and 70°F

The actual calibration for ammonia is then

$$(\text{SCFM})_{\text{NH}_3} = 2.38 \left(\frac{P_{\text{op}}}{14.7} \times \frac{530}{T_{\text{op}}} \right)^{1/2}$$

4. Hydrogen and helium flowmeter

Fisher & Porter Model No. 10A3565A

Serial No.: 7003E1195B1

Tube No.: Tri-flat FP-1/4-16-G-5/84

Float type: 1/4 CD (constant density glass)

Calibration curves were obtained using the procedure outlined in the F&P Tri-Flat Variable Area Flowmeter Handbook. A previously calibrated Precision Scientific Wet Test Meter (U. of H. Serial No. 68398) was used for this purpose.

The results for hydrogen and helium are shown in Figures I-2 and I-3 respectively.

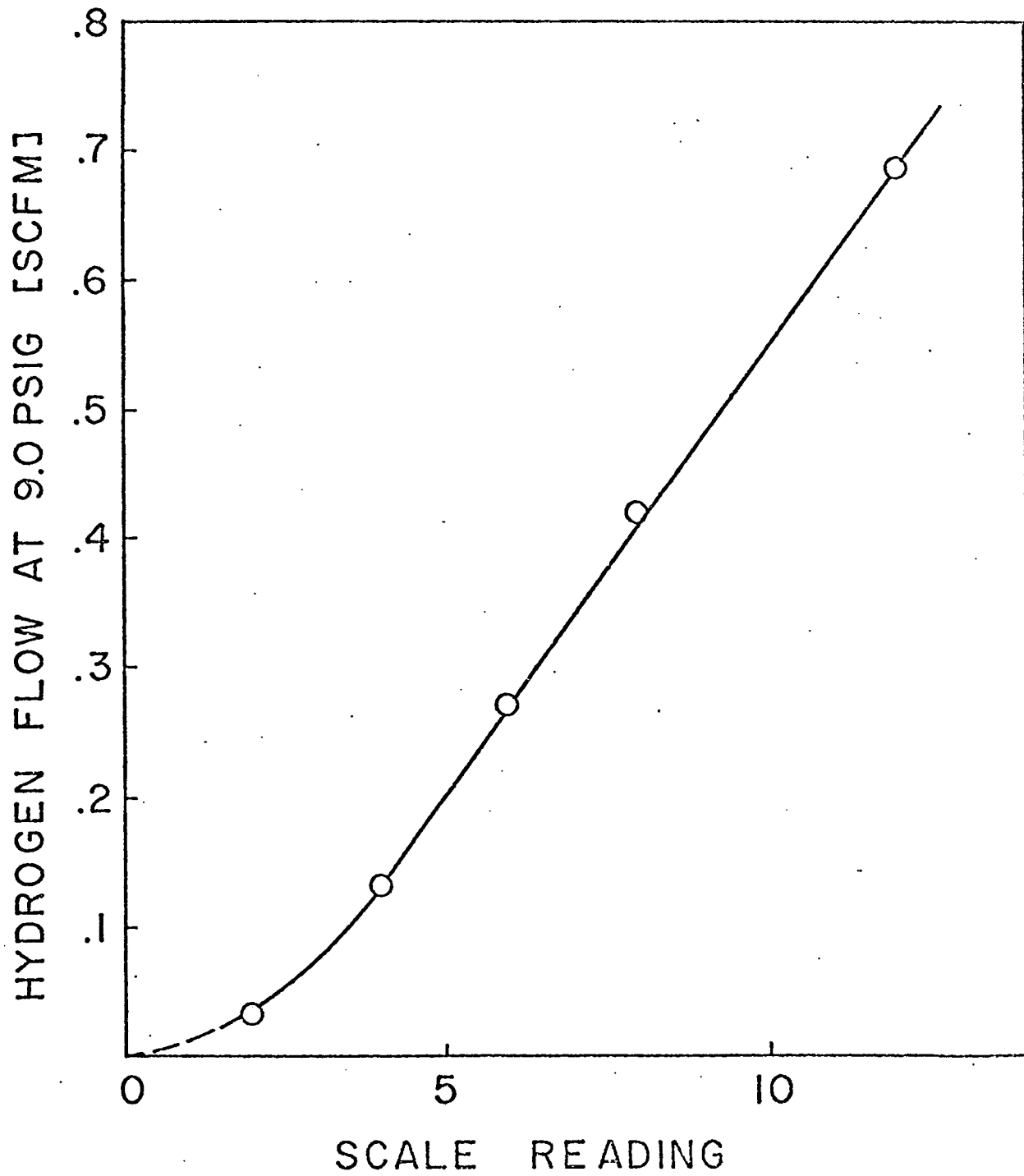


Figure I.2

Hydrogen flowmeter calibration (1/4 CD float)

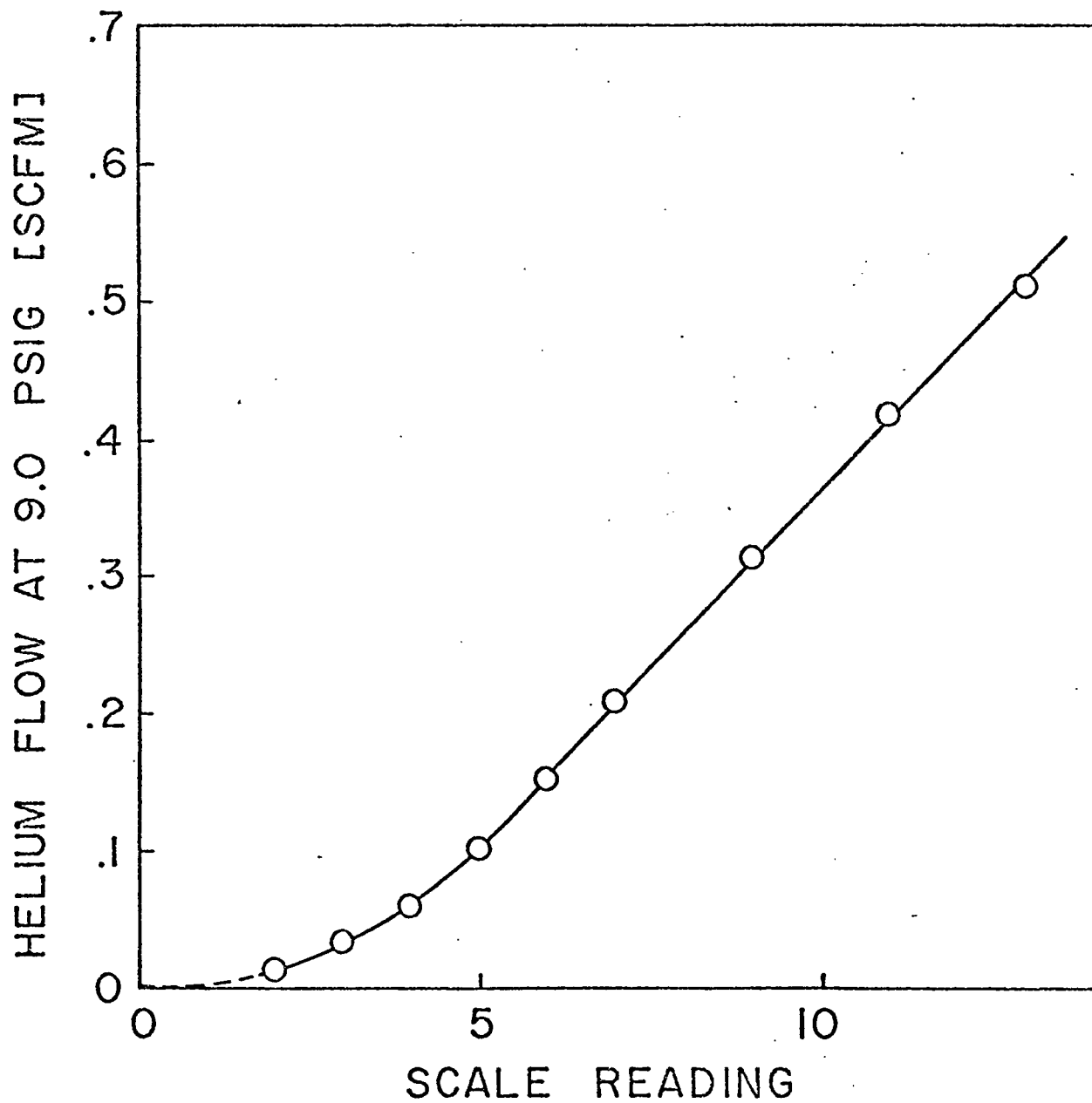


Figure I.3

Helium flowmeter calibration (1/4 CD float)

APPENDIX II

TURBULENCE INTENSITY MEASUREMENTS FOR CONSTANT TEMPERATURE OPERATION (HOT WIRE SENSOR)

In the theoretical section of this work, the following relation was derived for nonreacting wires operating at constant temperature.

$$\frac{2e_{\text{rms}}}{\langle E \rangle} = nf \frac{u'_{\text{rms}}}{\langle u \rangle} \quad (2-43)$$

where \underline{n} is the exponent of the velocity in King's equation and \underline{f} was defined as

$$f = \frac{B\langle u \rangle^n}{A + B\langle u \rangle^n} \quad (2-42)$$

Both \underline{n} and \underline{f} can be obtained experimentally.

The general relation between voltage and velocity in a turbulent flow field is given by King's equation

$$E_b^2 = K_1 + K_2 u^n \quad (4-3)$$

where E_b = output bridge voltage

u = velocity past the sensor

so that in principle, by operating the system at two different Reynolds numbers the value of the three constants in Eq. (4-3) can be determined.

The constant K_1 would be obtained from the intercept at zero velocity and n can be calculated from

$$\frac{(E_b^2)_2 - K_1}{(E_b^2)_1 - K_1} = \left(\frac{u_2}{u_1}\right)^n \quad (\text{II-1})$$

A better way to obtain the parameters in Eq.(2-43) is to run the system over a wide range of Reynolds numbers, measure E_b and the velocity for each case and to obtain the best least squares fit for the non-linear relation

$$E_b^2 = E_b^2 (u^n) \quad (\text{II-2})$$

This can be done using available non-linear least squares computer subroutines.

For the measurements, a TSI probe (model 1215 V) holding a P2 type sensor was connected to a constant temperature anemometer. The output bridge voltage was obtained for six different Reynolds numbers between 2000 and 8000. The relation obtained was

$$E_b^2 = 7.83 + 1.42 u_{\max}^{0.50} \quad (\text{II-3})$$

The rms deviation of the experimental points (E_b^2) about this

least squares line was 17%. The value of $n = 0.5$ is a generally accepted one for gases under most normal operation conditions.

Equation (2-43) can now be rewritten as

$$\frac{u'_{\text{rms}}}{\langle u \rangle} = \frac{4}{f} \frac{e_{\text{rms}}}{\langle E_b \rangle} \quad (\text{II-4})$$

In order to evaluate the factor f , Eq. (II-3), which relates the square of the voltage to the velocity, apparently needs to be changed to the form of Eq. (2-34) since A and B , and not K_1 and K_2 , are the constants that define f .

However, it can be shown that A and B are related to K_1 and K_2 respectively by a multiplication constant. This constant, F , depends on the surface area of the sensor, the total resistance of the assembly and the difference in temperature between the sensor and the environment. Hence,

$$\begin{aligned} K_1 &= FA \\ K_2 &= FB \end{aligned} \quad (\text{II-5})$$

Therefore, the factor f at a given Reynolds number can be expressed as

$$f = \frac{K_2 \langle u_m \rangle^{0.5}}{\langle E_b^2 \rangle} \quad (\text{II-6})$$

For this study most of the runs were done at $N_{Re} = 4000$.

Under these conditions

$$\langle E_b^2 \rangle = 11.28 \text{ volts}^2$$

$$K_2 = 1.42 / (30.48)^{1/2} \text{ volts}^2 / (\text{cm/sec})^{1/2}$$

$$\langle u_m \rangle = 178 \frac{\text{cm}}{\text{sec}}$$

yielding

$$f = 0.304$$

The turbulence intensity $u'_{rms} / \langle u \rangle$ at a channel Reynolds number of 4000 can be calculated from Eq. (II-4). The measured values for the E_b and e'_{rms} were

$$E_b = 3.35 \text{ v}$$

$$e'_{rms} = 0.028 \text{ v}$$

and therefore,

$$\frac{u'_{rms}}{\langle u \rangle} = 0.11$$

This is the same value obtained previously for this channel from standard hot film measurements.

APPENDIX III

DERIVATION OF EQUATION (2-16) AND EQUATION (2-56) WHEN THE LEWIS NUMBER IS DIFFERENT FROM UNITY

A) The Pseudo-Steady State Model

Under the assumptions of the pseudo-steady state, Chapter II (section B), Equations (2-1), (2-2) and (2-3) are reduced to the single differential equation:

$$\frac{A\rho C_p}{p} \frac{dT}{dt} = h(T_g - T) + (-\Delta H)k_c C_g \quad (\text{III-1})$$

Introducing fluctuating quantities for the temperatures, concentration and transport coefficients, Eq. (III-1) can be written as

$$\frac{A\rho C_p}{\langle T - T_g \rangle p \langle h \rangle} \frac{dT'}{dt} = \left(1 + \frac{h'}{\langle h \rangle}\right) \left(\frac{T'_g - T'}{\langle T - T_g \rangle} - 1\right) + \left(1 + \frac{k'_c}{\langle k_c \rangle}\right) \left(1 + \frac{C'_g}{\langle C_g \rangle}\right) \quad (\text{III-2})$$

The following relations were used in obtaining Eq. (III-2)

$$\frac{d\langle T \rangle}{dt} = 0$$

$$\frac{(-\Delta H) \langle k_c \rangle \langle C_g \rangle}{\langle h \rangle \langle T - T_g \rangle} = 1$$

Neglecting second order terms, Eq. (III-2) can be simplified to

$$\frac{\tau_o}{\langle \Delta T_{ad}^* \rangle} \frac{dT'}{dt} = \frac{T'_g}{\langle \Delta T_{ad}^* \rangle} - \frac{T'}{\langle \Delta T_{ad}^* \rangle} + \frac{C'_g}{\langle C_g \rangle} + \frac{k'_c}{\langle k_c \rangle} - \frac{h'}{\langle h \rangle} \quad (\text{III-3})$$

where

$$\tau_o = \frac{A\rho C_p}{p\langle h \rangle}$$

$$\langle \Delta T_{ad}^* \rangle = \langle T - T_g \rangle$$

Defining

$$\theta'_w = \frac{T'}{\langle \Delta T_{ad}^* \rangle}$$

$$\theta'_g = \frac{T'_g}{\langle \Delta T_{ad}^* \rangle}$$

$$c' = \frac{C'_g}{\langle C_g \rangle}$$

and rearranging, we obtain from Eq. (III-3)

$$\tau_o \frac{d\theta'_w}{dt} + \theta'_w = \theta'_g + c' + \frac{k'_c}{\langle k_c \rangle} - \frac{h'}{\langle h \rangle} \quad (\text{III-4})$$

For flow of a fluid at right angles to a cylinder, the average heat transfer coefficient is given by [15]

$$N_u = \frac{hd}{k_f} = 0.43 + 0.532 Re^{0.5} Pr^{0.31} \quad (\text{III-5})$$

The analogous expression for the mass transfer coefficient would be

$$Sh = \frac{k_c d}{D_{AB}} = 0.43 + 0.532 Re^{0.5} Sc^{0.31} \quad (\text{III-6})$$

From Eqs. (III-5) and (III-6) it can be shown that

$$\frac{h}{\langle h \rangle} = 1 + N_2 \frac{u'}{\langle u \rangle} \quad (\text{III-7})$$

and

$$\frac{k_c}{\langle k_c \rangle} = 1 + N_1 \frac{u'}{\langle u \rangle} \quad (\text{III-8})$$

where

$$N_1 = \frac{0.532 (Sc^{0.31}) \langle Re_w^{.5} \rangle}{2 \langle Sh \rangle} \quad (\text{III-9})$$

$$N_2 = \frac{0.532 (Pr^{0.31}) \langle Re_w^{.5} \rangle}{2 \langle N_u \rangle} \quad (\text{III-10})$$

so that

$$\frac{N_1}{N_2} = (N_{Le}^{0.31}) \frac{\langle N_{Nu} \rangle}{\langle N_{Sh} \rangle} \quad (\text{III-11})$$

Since

$$h = \langle h \rangle + h' \quad (III-12)$$

$$k_c = \langle k_c \rangle + k'_c$$

from Eq. (III-7) and (III-8)

$$\frac{h'}{\langle h \rangle} = N_2 \frac{u'}{\langle u \rangle} = N_2 U' \quad (III-13)$$

$$\frac{k'_c}{\langle k_c \rangle} = N_1 \frac{u'}{\langle u \rangle} = N_1 U' \quad (III-14)$$

Substitution of Eq. (III-13) and (III-14) into Eq. (III-4), yields

$$\tau_o \frac{d\theta'_w}{dt} + \theta'_w = \theta'_g + C' + (N_1 - N_2) U' \quad (III-15)$$

Numerical calculations

For a 0.075 mm diameter wire, at $N_{re} = 4000$, it can be shown experimentally that

$$T_c \approx 1.28 \bar{T}_w$$

Assuming a $\bar{T}_{max} \approx 490^\circ\text{C}$ for operation with H_2 - air mixtures, and $T_g = 24^\circ\text{C}$, this gives

$$\bar{T}_w \approx 383^\circ\text{C}$$

From Reference [16], we have at $\bar{T}_w \approx 721^\circ\text{F}$

$$v_{\text{air}} = 0.596 \text{ cm}^2/\text{sec}$$

$$v_{\text{H}_2} = 4.080 \text{ cm}^2/\text{sec}$$

For $T_g = 75^\circ\text{F}$

$$v_{\text{air}} = 0.155 \text{ cm}^2/\text{sec}$$

$$v_{\text{H}_2} = 1.080 \text{ cm}^2/\text{sec}$$

If $x_g = 0.025$

$$\bar{v}_{\text{mix}} = \bar{v}_{\text{air}} (.975) + \bar{v}_{\text{H}_2} (.025)$$

$$\bar{v}_{\text{air}} = (0.596 + 0.155)/2$$

$$\bar{v}_{\text{air}} = 0.375 \text{ cm}^2/\text{sec}$$

$$\bar{v}_{\text{H}_2} = (4.080 + 1.080)/2$$

$$\bar{v}_{\text{H}_2} = 2.580 \text{ cm}^2/\text{sec}$$

Hence

$$\bar{v}_{\text{mixt}} = 0.375 \times .975 + 2.580 \times 0.025$$

$$\bar{v}_{\text{mix}} = 0.430 \text{ cm}^2/\text{sec}$$

At a channel $N_{Re} = 4000$

$$\langle u_{\max} \rangle = 178 \text{ cm/sec}$$

or

$$\langle Re_w \rangle = \frac{\langle u_m \rangle d_w}{\bar{v}_{\text{mix}}} = 3.10$$

From Reference [17] the following data is obtained

substance	ϵ/k ($^{\circ}\text{K}$)
H_2	59.7
air	78.6

$$\epsilon_{AB}/k = (78.6 \times 59.7)^{1/2} = 68.50^{\circ}\text{K}$$

Besides, at 293°K [17]

$$D_{AB}P = 7.701 \times 10^5 \text{ dyn/sec}$$

Assuming $P = 1.013 \times 10^6 \text{ dyn/cm}^2$

$$D_{AB} = 0.76 \text{ cm}^2/\text{sec at } 293^{\circ}\text{K}$$

For $\bar{T}_w \approx 656^\circ\text{K}$

$$\frac{kT}{\epsilon_{AB}} = 9.57$$

and $\Omega_D = 0.7480$

At reference temperature (293°K)

$$\frac{kT}{\epsilon_{AB}} = 4.28$$

and $\Omega_D = 0.8703$

then

$$D_{AB}(656^\circ\text{K}) = 0.76 \left(\frac{656}{293}\right)^{3/2} \left(\frac{0.8703}{0.7480}\right) = 2.96 \frac{\text{cm}^2}{\text{sec}}$$

At

$$T_g = 297^\circ\text{K}$$

$$\frac{kT}{\epsilon_{AB}} = 4.33$$

$$\Omega_D = 0.8681$$

Hence,

$$D_{AB}(297^\circ\text{K}) = 0.76 \left(\frac{297}{293}\right)^{3/2} \left(\frac{0.8703}{0.8681}\right) = 0.78 \frac{\text{cm}^2}{\text{sec}}$$

$$\bar{D}_{AB} = 1.87 \text{ cm}^2/\text{sec}$$

Therefore,

$$N_{Sc} = \frac{\bar{v}}{\bar{D}_{AB}} = \frac{0.430}{1.87} = 0.23$$

From Ref. [16] we obtain

$$\text{at } \bar{T}_w = 721^\circ\text{F}$$

$$N_{Pr}(\text{air}) = 0.682$$

$$N_{Pr}(\text{H}_2) = 0.659$$

$$N_{Pr}(721^\circ\text{F}) = 0.681 \text{ (mixture)}$$

At $T_g = 75^\circ\text{F}$

$$N_{Pr}(\text{air}) = 0.709$$

$$N_{Pr}(\text{H}_2) = 0.705$$

$$N_{Pr}(75^\circ\text{F}) = 0.709 \text{ (mixture)}$$

Therefore,

$$\bar{N}_{Pr} = 0.695$$

Substitution of these values in Eq. (III-5) and (III-6) along with Re_w yields,

$$\langle N_{Nu} \rangle = 1.267$$

$$\langle N_{Sh} \rangle = 1.024$$

We now evaluate N_1 and N_2 from Eq. (III-9) and (III-10). The results are

$$N_1 = 0.2899$$

$$N_2 = 0.3302$$

Therefore, $(N_1 - N_2) \approx -0.040$.

If the gas temperature does not fluctuate, (III-15) becomes

$$\tau_o \frac{d\theta'_w}{dt} + \theta'_w = C' - 0.040 U' \quad (\text{III-16})$$

For a channel Reynolds number of 4000, the quantity U' is of the order of 0.10. Moreover, C' was found to vary in these experiments between 0.03 and 0.15. This means that, in the worst case, the second term in the rhs of Eq. (III-16) is about

13% of C' and therefore in general it may be neglected.

This gives,

$$\tau_o \frac{d\theta'_w}{dt} + \theta'_w = C' \quad (\text{III-17})$$

which is identical to Eq. (2-16) derived in Chapter II for N_{Le} equal to unity.

B. Constant temperature method with reaction

The following relation was derived in Chapter II for the case of a mass-transfer controlled reaction occurring on the surface of an electrically heated wire:

$$\frac{h}{\langle h \rangle} \left(\frac{T_w - T_g}{T_w^* - T_g} \right) = \frac{k_c}{\langle k_c \rangle} \frac{C_g}{\langle C_g \rangle} + \frac{JI^2 R_w}{Pl_w \langle h \rangle (T_w^* - T_g)} \quad (\text{III-18})$$

Introducing fluctuating quantities for h , k_c , C_g and I ,

Equation (III-18) becomes

$$\left(1 + \frac{h'}{\langle h \rangle} \right) \left(\frac{T_w - T_g}{T_w^* - T_g} \right) = \left(1 + \frac{k'_c}{\langle k_c \rangle} \right) \left(1 + \frac{C'_g}{\langle C_g \rangle} \right) + \frac{J \langle I \rangle^2 \left(1 + \frac{i}{\langle I \rangle} \right)^2 R_w}{Pl_w \langle h \rangle (T_w^* - T_g)} \quad (\text{III-19})$$

Define

$$m \equiv \frac{T_w^* - T_g}{T_w - T_w^*}$$

and note that

$$\frac{J\langle I \rangle^2 R_w}{\langle h \rangle P \ell_w (T_w - T_w^*)} = 1 \quad (2-48)$$

Equation (III-19) becomes, after neglecting second order terms,

$$\left(1 + \frac{h'}{\langle h \rangle}\right) \left(\frac{m+1}{m}\right) = 1 + \frac{C'_g}{\langle C'_g \rangle} + \frac{k'_c}{\langle k'_c \rangle} + \frac{1}{m} \left(1 + 2\frac{i}{\langle I \rangle}\right) \quad (III-20)$$

It was shown in Section A of this Appendix that when $N_{Le} \neq 1$ the following is valid

$$\frac{k'_c}{\langle k'_c \rangle} = N_1 U' \quad (III-14)$$

$$\frac{h'}{\langle h \rangle} = N_2 U' \quad (III-13)$$

Combining these equations yields,

$$\frac{k'_c}{\langle k'_c \rangle} = \left(\frac{N_1}{N_2}\right) \frac{h'}{\langle h \rangle} \quad (III-21)$$

Substitution of (III-21) into (III-20) gives, after rearrangement,

$$\frac{h'}{\langle h \rangle} \left[1 + m\left(1 - \frac{N_1}{N_2}\right)\right] = mC' + \frac{2i}{\langle I \rangle} \quad (III-22)$$

Introduction of Eq. (2-38)

$$\frac{h'}{\langle h \rangle} = n f \frac{u'}{\langle u \rangle}$$

into (III-22) yields,

$$\alpha f n U' - m C' = \frac{2e}{\langle E \rangle} \quad (\text{III-23})$$

where

$$\alpha = \left[1 + m \left(1 - \frac{N_1}{N_2} \right) \right] \quad (\text{III-24})$$

Squaring (III-23) and time averaging, results

$$\left\langle \left(\frac{2e}{\langle E \rangle} \right)^2 \right\rangle = \langle (\alpha f n U')^2 \rangle - 2 \alpha m n f \langle U' C' \rangle + m^2 \langle (C')^2 \rangle \quad (\text{III-25})$$

If the value of n is taken as 0.5, Equation (III-25) can be rearranged to the following form

$$y = a + b x \quad (\text{III-26})$$

with

$$y = \frac{100}{m} \left[\frac{\langle (20e)^2 \rangle}{\langle E \rangle^2} - \frac{\alpha^2 \langle (5f u')^2 \rangle}{\langle u \rangle^2} \right] \quad (\text{III-27})$$

$$x = \frac{m}{10} \quad (\text{III-28})$$

$$a = -10^4 \alpha \langle fU'C' \rangle = -10^4 R_{uc} f \frac{u'_{rms}}{\langle u \rangle} \frac{c'_{rms}}{\langle C'_g \rangle} \quad (\text{III-29})$$

$$b = 10^5 \langle C'^2 \rangle \quad (\text{III-30})$$

Operation of the system at minimum of three different values of m , provides adequate data to construct the linear graph of y vs. x needed to determine C' and R_{uc} .

The value of U' , however, must be known in order to calculate y from Eq. (III-27). This quantity can be obtained during a separate measurement at constant temperature and no reaction. Under these conditions

$$m = 0 \quad (\text{Eq. 2-54})$$

and

$$\alpha = 1 \quad (\text{Eq. III-24})$$

Eq. (III-25) then becomes

$$\frac{2e_{rms}}{\langle E \rangle} = f_n \frac{u'_{rms}}{\langle u \rangle} \quad (2-43)$$

as before.

To obtain the velocity-concentration cross correlation, R_{uc} , the y vs x curve is extrapolated to $x = 0$. This is equivalent to $m = 0$ (Eq. III-28)

Equation (III-29) then becomes,

$$a = -10^{-4} R_{uc} f \frac{u'_{rms}}{\langle u \rangle} \frac{c'_{rms}}{\langle C_g \rangle} \quad (\text{III-29a})$$

As can be seen from Eq. (III-24), the value of α is equal or greater than one and increases linearly with m . If the value of N_1 and N_2 calculated in part A of this Appendix, are taken as typical for the conditions of these experiments, we obtain

$$\alpha = 1 + m \times 0.122 \quad (\text{III-31})$$

A typical value for m , in order to have reliable data ($\Delta R > 1$) is about 3 - 4. Therefore

$$\alpha \approx 1.40$$

and

$$\alpha^2 \approx 1.96 \approx 2$$

A typical minimum value ($\phi = 180^\circ$) for the first term in the brackets of Eq. (III-27) is

$$\frac{\langle (20e')^2 \rangle}{\langle E \rangle^2} \approx 1.5$$

On the other hand,

$$\frac{\langle (5fu')^2 \rangle}{\langle u \rangle^2} \approx 0.025$$

and the second term becomes,

$$\frac{\alpha^2 \langle (5fu')^2 \rangle}{\langle u \rangle^2} \approx 0.050$$

Therefore, the exclusion of the factor α^2 results in an overestimation of y by less than 2%.